Adsorptive Exclusion of Lead and Chromium from Tannery Wastewater Using MgO Impregnated Biochar Derived from Co-Pyrolysis of Banana Peel and Rice Husk

By

Tayyaba Kanwal

(Registration No: 00000400409)

A thesis submitted to National university of Science and Technology, Islamabad in partial fulfillment of the requirements for the degree of

Master of Science in

Environmental Engineering

Supervisor: Dr. Muhammad Ali Inam

Institute of Environmental Science and Engineering

School of Civil and Environmental Engineering

National University of Sciences and Technology (NUST)

Islamabad, Pakistan

(2024)

Approval Certificate

Certified that the contents and form of the thesis entitled

"Adsorptive Exclusion of Lead and Chromium from Tannery Wastewater Using MgO Impregnated Biochar Derived from Co-Pyrolysis of Banana Peel and Rice Husk"

Submitted by

Ms. Tayyaba Kanwal

Has been found satisfactory for partial fulfillment of the requirements of the degree of Master of Science in Environmental Engineering.

Dr. Rashid Iftikhar
Assistant Professor
IESE (SCEE) NUST Islamabad

Supervisor: ....

Assistant Professor

Dr. Muhammad Ali Inam
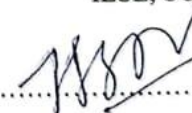
IESE, SCEE, NUST

GEC Member: ....

Dr. Rashid Iftikhar

Assistant Professor

IESE, SCEE, NUST

GEC Member: ....

Dr. Hassan Anwer

Assistant Professor

IESE, SCEE, NUST

GEC Member: ....

Dr. Muhammad Bilal Khan Niazi

Professor

SCME, NUST

Acceptance Certificate

It is certified that final copy of MS/MPhil Thesis written by Ms. Tayyaba Kanwal (Registration No: 00000400409) of SCEE (IESE) has been vetted by the undersigned, found complete in all respects as per NUST Statues/Regulations, is free of plagiarism, errors, and mistakes, and is accepted as partial fulfillment for the award of MS/MPhil degree. It is further certified that necessary amendments as pointed out by GEC members of the scholar have also been incorporated in the said thesis.

Supervisor: _____

Dr. Rashid Iftikhar
Assistant Professor
IESE (SCEE) NUST Islamabad

Dated: 27.12.2024

Dr. Hassan Anwer
Assistant Professor
HoD Environmental Engineering
SCEE (IESE), NUST
H-12 Islamabad

Head of Department: _____

Dated: 27.12.2024

Associate Dean _____

PROF DR MUHAMMAD ARSHAD
Associate Dean SCEE (IESE)
NUST H/12. Islamabad

Dated: 31.12.2024

Principal & Dean SCEE _____

Dated: 31 DEC 2024

PROF DR MUHAMMAD IRFAN
Principal & Dean
SCEE, NUST

ii

Declaration Certificate

I declare that this research work titled "**Adsorptive Exclusion of Lead and Chromium from Tannery Wastewater Using MgO Impregnated Biochar Derived from Co-Pyrolysis of Banana Peel and Rice Husk** "is my own work. The work has not been presented elsewhere for assessment. The material that has been utilized from other sources has been properly acknowledged/referred.

Tayyaba Kanwal

00000400409

CERTIFICATE FOR PLAGIARISM

It is certified that MS Thesis title "Adsorptive Exclusion of Lead and Chromium from Tannery Wastewater Using MgO Impregnated Biochar Derived from Co-Pyrolysis of Banana Peel and Rice Husk" by Regn no. 00000400409 Name: (400409) Tayyaba Kanwal has been examined by us. We undertake the following:

a. Thesis has significant new work/knowledge as compared to that already published or are under consideration to be published elsewhere. No sentence, equation, diagram, table, paragraph or section has been copied verbatim from previous work unless it is placed under quotation marks and duly referenced.

b. The work presented is original and the own work of the author (i.e. there is no plagiarism). No ideas, processes, results, or words of others have been presented as author's own work.

c. There is no fabrication of data or results which have been analyzed.

d. There is no falsification by manipulating research materials, equipment, or processes, or changing or omitting data or results such that the research is not accurately represented in the research record.

e. The thesis has been checked using TURNITIN (Copy of originality report attached) and found within limits as per HEC Plagiarism Policy and instructions issued from time to time.

Signature of Supervisor: _____

Name of Supervisor: Dr. Muhammad Ali Inam

Dated: 27/12/24

DEDICATION

I dedicate this research work to my loving parents and siblings. Their unwavering love, encouragement, and guidance have been my strength at every step of this journey. I am profoundly grateful for their invaluable presence in my life.

ACKNOWLEDGEMENT

I begin with gratitude to Allah for His boundless mercy and guidance. I also pay respectful tribute to the Holy Prophet Muhammad (S.A.W.), whose noble life remains a timeless source of inspiration.

My sincere appreciation goes to my supervisor, Dr. Muhammad Ali Inam, for his exceptional guidance, support, and mentorship throughout my research journey. His encouragement and expertise have profoundly impacted my work.

I am grateful for the valuable guidance and feedback from the GEC and acknowledge the support from lab staff.

Finally, I am deeply grateful to my family for their support and encouragement, which have been the cornerstone of my journey, making the completion of my master's degree possible.

Tayyaba Kanwal

TABLE OF CONTENTS

LIST OF ABBREVIATION

RHBC   Rice Husk Biochar

BPBC   Banana Peel Biochar

CBC   Combined Biochar

MgO@RHBC   Magnesium Oxide Modified Rice Husk Biochar

MgO@BPBC   Magnesium Oxide Modified Banana Peel Biochar

MgO@CBC   Magnesium Oxide Modified Combined Biochar

RBCs   Raw Biochars

MgO@BCs   Magnesium Oxide Modified Biochars

AR:MgO@CBC$_{Cr}$ Cr Loaded MgO Modified Combined Biochar

AR:MgO@CBC$_{Pb}$ Pb Loaded MgO Modified Combined Biochar

AR:MgO@CBC$_{Cr-Pb}$ Cr & Pb Loaded MgO Modified Combined Biochar

SEM   Scanning Electron Microscope

EDX   Energy Dispersive X-ray

XRD   X-ray Diffraction

FT-IR   Fourier Transform Infrared Spectroscopy

BET   Brunauer Emmett Teller

SS   Single Solute System

BS   Binary Solute System

LIST OF TABLES

LIST OF FIGURES

ABSTRACT

Heavy metal contamination from tannery effluents poses a significant threat to human health, wildlife, and the environment, necessitating effective and sustainable removal methods to mitigate this pollution. This study evaluated MgO-impregnated biochar (MgO@BC), synthesized from the co-pyrolysis of rice husks and banana peels, for the simultaneous removal of Pb (II) and Cr (VI) from effluents in both single solute and binary solute system. The physicochemical properties of the materials were comprehensively characterized through a multi-technique approach, encompassing X-ray diffraction, BET analysis, FTIR spectroscopy, SEM-EDX, and proximate analysis, to determine their structural, morphological, and textural attributes. In single solute system the results revealed that MgO@CBC achieved remarkable removal efficiencies of 94% for Cr (VI) at pH 2 and 100% for Pb (II) at pH 4, using a dosage of 2 g/L and an initial concentration of 20 mg/L. In binary solute systems, under the same initial concentration and dosage conditions, pH 2, Cr (VI) removal was 88.5% and Pb (II) removal was 99%. Notably, a synergistic effect was observed in the combined system at pH 2, wherein the enhanced removal efficiency of Pb (II) was facilitated by the surface properties and charge neutralization processes of MgO@CBC. The isotherm study found out that binary solute system data conform more closely to langmuir and freundlich models than the single solute system. Post-removal FTIR and XRD analyses suggest that charge neutralization, surface complexation, and metal ion exchange are the key mechanisms governing Pb (II) and Cr (VI) removal by MgO@CBC. Furthermore, MgO@CBC demonstrated recyclability over five regeneration cycles, with a gradual decline in removal efficiency (Pb (II) and Cr (VI)) due to active site deactivation and surface degradation. The results confirm its potential as a reusable adsorbent with active MgO sites for effective multi-metal removal from industrial wastewater.

CHAPTER 1

INTRODUCTION

1.1. Background

Environmental pollution is a global challenge affecting developed and developing states, worsened by growing populations and industrialization, thereby contributing substantially to global contamination (Nasrollahi et al. 2020). The growing need for resources and industrial expansion leads to the contaminant discharge into water bodies, posing risks to the quality of water. Human activities, including municipal, industrial, and domestic farming activities, have a worldwide influence by producing wastewater and acting as major environmental stressors. Pesticides, chemicals, fertilizers, heavy metals, non-biodegradable substances, bioaccumulating nutrients, microbes, and hazardous compounds contribute to the pollution of soil and water systems (Rathi et al. 2021). The rising levels of these pollutants remain inadequately controlled by national or international regulations, raising environmental concerns. Society faces the immense challenge of addressing these issues, struggling with the urgent need for extensive and effective solutions (Akhtar et al. 2021).

Water, comprised of approximately 75% of the earth's crust and essential for life, has deteriorated due to the discharge of industrial, agricultural, and residential pollutants (Noreen et al. 2019). The World Wildlife Fund predicts that by 2025, two-thirds of the global population could confront water scarcity, posing risks to human health and agriculture (WWF Pakistan-water Scarcity). In Pakistan, severe water scarcity, with per capita water availability dropping from 5,000 m³ in 1947 to 930 m³ today and projected to fall to 860 m³ by 2025, exacerbates the critical public health challenge posed by contaminated water (Ishaque et al. 2023).

Heavy metal contamination in aquatic bodies, considered a major global concern with ecotoxicological and health implications (H. Yu et al., 2021), has been increasing in recent years due to rapid population growth and industrial expansion (Qayoom et al., 2022). Heavy metals have received special attention due to their toxicity, bioaccumulation, and long-term effects (Dash, Borah, and Kalamdhad 2021a). These persistent metals are dangerous because they don't break down over time, becoming hazardous when concentrations reach permitted limits (Dash, Borah, and Kalamdhad 2021b).

Lead, nickel, and chromium are commonly present in industrial effluent originating from diverse sectors such as metal plating, mining, smelting, battery manufacturing, tanneries, petroleum refining, paint, pesticides, pigment, printing, and photography (Abu Sayid et al. 2020). Particularly, tannery industries extensively employ metals like Cr, Cu, Ni, Cd, and Pb, known for their comparable toxicity (Hossain et al. 2021). As the tannery industry expands, tannery effluent emerges as a major source of industrial pollution (C. Zhao and Chen et al. 2019). The prevalent chrome-tanning technique employed by tanneries globally aims to produce high-quality leather with a consistent texture (Younas et al. 2022). However, this process contributes to the release of tannery wastewater, posing environmental and human health risks (Moradi and Moussavi 2019). The characteristics of tannery wastewaters encompass chromium, sulphur, nitrogenous chemicals, organic and inorganic debris, high salinity levels, and suspended and dissolved particles (Alemu et al. 2016).

Chromium, particularly Cr (VI), poses a significant risk in the tannery sector due to its high toxicity and carcinogenicity (Y. Zhao et al. 2017). In tannery industrial effluent, Cr occurs in trivalent (Cr^{3+}) and hexavalent (Cr^{6+}) forms, with Cr^{6+} being extremely mobile and poisonous (Ahmad et al. 2020). However, leather cannot fully use Cr salts, resulting in polluted tannery effluent (Younas et al. 2022). Chromate-rich tannery effluent contaminates the food chain and harms animals, humans, and the environment (Younas et al. 2022). When metal concentrations in wastewater exceed allowable limits, they pose serious threats to both human health and the environment. The hexavalent form of chromium, specifically associated with the development of lung cancer (Shrestha et al. 2021a), poses carcinogenic risks to humans. Elevated chromium levels can lead to skin irritations, respiratory problems, ulcers, anemia, and damage to the male reproductive system (Shukla, Mahmood, and Singh 2021). The WHO outlined allowable limits of less than 0.05 mg/L Cr ions in drinking water and 0.05 mg/L in effluent for the protection of human health (Usmani et al. 2023;Shrestha et al. 2021b). According to the United States Environmental Protection Agency (USEPA), the maximum allowable level of total Cr for drinking water is 0.1 mg/L, respectively. Lead (II) accumulation in bones causes bone problems and adversely affects both the central and peripheral neurological systems (Shrestha et al. 2021a). In addition to causing various metabolic and physiological issues in people, animals, and plants, lead (II) has a significant potential for toxicity, mutagenicity, and cancer (V. Kumar, Dwivedi, and Oh 2022a). For Pb (II), the World Health Organization (WHO) recommends a safe level of less than 0.01 mg/L in reservoirs of drinking water and 0.01 mg/L in effluent (Y. Zhang and Duan 2020). Research underscores the extreme significance of lead and chromium

contamination, emphasizing the urgent need for comprehensive addressing to prevent potential catastrophic events (Nithya and Sudha 2017).

1.2. Overview of Chromium

Derived from the Greek word "chroma," Chromium (Cr) stands as the earth's 24th most abundant element, recognized as a hard, silvery transition metal with the symbol Cr and atomic number 24. Existing in the environment as Cr^{6+} and Cr^{3+}, chromium takes various forms, including CrO_4^{2-}, $HCrO_4^{-}$, and $Cr_2O_7^{2-}$, in both aquatic and terrestrial habitats (Younas et al. 2022; Novak et al. 2018). The trivalent form of chromium, Cr (III), is non-toxic, usually found in food and nutritional supplements. In comparison, the hexavalent form of chromium, Cr (VI), is less common and more toxic when detected in industrial effluent, known to possess carcinogenic properties (Hayashi et al. 2021). Therefore, exposure to Cr (VI), even at low amounts, poses a significant risk, thereby a global challenge for researchers working on removal techniques.

1.2.1. Uses of Chromium

Chromium is extensively utilized in the production of steel and various alloys, forming the backbone of applications in chrome plating, dye and pigment manufacturing, leather and wood preservation, and the treatment of cooling tower water (Verger et al. 2018). Moreover, smaller quantities of chromium find application in drilling muds, textiles, and toner for photocopying machines (Shadreck and Mugadza 2013). The broad usage of chromium across diverse industrial processes, including pigment manufacturing, leather tanning, and chromate coating, raises concerns about potential environmental contamination (Hayashi et al. 2021).

1.2.2. Sources of Chromium

Chromium is a naturally occurring element that occurs in various environmental components such as rocks, plants, soil, volcanic dust and gas. These industries encompass cement plants, electroplating, steel production, paints, pigments, dye manufacturing, wood and leather preservation, metal plating, timber processing, paper and pulp production, oxidative dyeing, and tobacco smoke. Chromium (VI) can also leach from unsanitary landfills (Sajad et al. 2020). Atmospheric chromium load is contributed by various sectors, including ore refining, chemical and refractory processing, cement production, vehicle brake lining, catalytic converters, leather tanning, and chrome pigments (Younas et al. 2022). Chromium enters the atmosphere through smoke, emissions from automotive catalytic converters, coal combustion. Moreover, accidental

spills during the handling, storage, and transportation of chromium-based products can lead to its discharge into the surrounding water bodies and soil (Poznanović Spahić et al. 2019).

1.2.3. Potential exposure of Chromium

Exposure to the public occurs through ingestion of chromium-containing water, inhalation of affected air and food consumption. Moreover, exposure via the skin occurs when using consumer products such as leather tanned with chromic sulphate or wood treated with copper dichromate (M. Zhao et al. 2020). Occupational exposure is common when working in tanning industries, steel manufacturing and chrome plating industries. People residing near chromium waste disposal sites are more likely to experience chromium exposure (H. Sun, Brocato, and Costa 2015).

1.2.4. Impacts of Chromium

Overexposure of Chromium (VI) may result in gastrointestinal problems in humans and animals causing stomach discomfort and vomiting. Inhalation of compounds containing hexavalent chromium (Cr VI) can result in a range of health issues, including nasal septum perforation, bronchitis, asthma, pneumonitis, pharyngitis, and liver problems (Sharma et al. 2020). Notably, there is an elevated risk of bronchial cancer associated with inhalation, in contrast to the effects observed with dermal or oral exposure. Cr (VI) amount in the atmosphere and its duration of exposure have been connected to the incidence and risk of cancer-related death. Given that the skin is the body's primary organ and is believed to undergo some biotransformation, dermal contact with Cr can lead to skin corrosion, dermatitis, eczema, ulcers, and allergic skin responses (Alvarez et al. 2021).

1.3. Overview of Lead

The symbol Pb, denoting lead, is derived from the Latin word "plumbum." It is a soft, silvery-white, or grayish metal situated in Group 14 (IVa) of the periodic table, with an atomic number of 82 and a relative atomic mass of 207.2, belonging to the p-block. The electron configuration is [Xe] $4f^{14}$, $5d^{10}$, $6s^2$, $6p^2$. Lead compounds typically exhibit oxidation states of +2 or +4 (V. Kumar et al. 2022b). Notable lead compounds include lead monoxide (PbO) in the +2 state, lead dioxide (PbO_2) in the +4 state, and tri-lead tetroxide (Pb_3O_4) (Sk and Chattopadhyay 2022). Despite its exceptional malleability, ductility, and density, lead is a poor conductor of electricity. As a naturally occurring toxic metal in the earth's crust. Its widespread use has led to extensive environmental contamination, human exposure, and significant public health problems worldwide (Jumina et al. 2020).

1.3.1. Sources and pathways of Lead exposure

Lead exposure occurs through both occupational and environmental sources, primarily from inhaling lead particles during activities like smelting, recycling, and paint striping, as well as using lead aviation fuel. Additionally, ingestion of lead-contaminated dust, water from lead pipes, and food from lead-glazed or lead-soldered containers contributes to exposure. Hand-to-mouth behavior further compounds the risk. Young children, who absorb 4-5 times more lead than adults, are particularly vulnerable to lead poisoning. Once in the body, lead is distributed to organs such as the brain, kidneys, liver, and bones, where it accumulates over time. The stored lead in bones may be released into the blood during pregnancy, posing a risk to the growing fetus (Nag and Cummins 2022). Undernourished children, lacking essential nutrients like calcium or iron, are more susceptible to lead absorption. The highest risk is for the young, as their developing nervous systems are particularly vulnerable during this stage (Huang et al. 2024).

1.3.2. Uses of Lead

Lead (Pb) finds widespread use due to its low melting point (327.462^0C), ductility, high density, and relative inertness to oxidation states. Employed in pipes, paint, pigments, pewter, and lead-acid batteries, it resists corrosion. Additionally, lead serves roles in leaded gasoline, fusible alloys, ionizing radiation shielding, lead crystal glasses (containing 12–28% lead oxide), and solder for electrical devices (V. Kumar et al. 2022b). Particularly, most of the globally consumed lead contributes to the production of lead-acid batteries for automobiles. Beyond this, lead is integral to various items such as leather, solder, stained glass, ammunition, ceramic glazes, jewelry, and toys, among others (Bouida et al. 2022).

1.3.3. Effects of Lead

Lead (Pb) poses a severe threat to various body systems, including the immunological, skeletal, circulatory, enzymatic, neurotoxic, neurological, and endocrine systems (Hossain et al. 2021). Exposure to lead has particularly dire consequences for children, leading to severe damage to the brain and central nervous system, potentially resulting in coma, convulsions, and death at high levels of exposure. Surviving children may experience permanent intellectual disabilities and behavioral disorders. Even at lower levels of exposure with no obvious symptoms, lead produces a spectrum of injuries across multiple body systems (A. Kumar et al. 2020). Pb (II) pollution negatively impacts land and water ecosystems due to its poisonous and carcinogenic properties. The toxicity of lead primarily arises from the generation of reactive oxygen species (ROS) within cells, causing oxidative stress and damaging membrane lipids, proteins, DNA,

and other macromolecules, disrupting cell function (Witkowska, Słowik, and Chilicka 2021). Lead inhibits enzymatic performance by substituting cationic species in enzymes, disrupting overall metabolic action. In the blood, it blocks heme production and damages the membranes of red blood cells (RBCs) and erythrocytes, leading to hemolysis and anemia. Lead poisoning significantly affects the peripheral nervous system (PNS) in adults and the central nervous system (CNS) in children. The impact extends to plants, affecting nutrient intake, water relations, and reducing photosynthetic activity, growth, development, and agricultural yield (V. Kumar, Dwivedi, and Oh 2022b). Pb (II) and its compounds present substantial health risks, disrupting ecosystems and impacting both flora and fauna. Removing Pb (II) from industrial effluent poses a challenge for industrialists, environmentalists, government agencies, and politicians concerned with health and the environment (V. Kumar, Dwivedi, and Oh 2022b). These hazardous chemicals, when entering water bodies, not only pollute the water but also directly harm waterborne microbes and pose a threat to human health through aquatic products. It is therefore imperative to implement suitable and affordable approaches to lower their concentrations or control their presence and movement in wastewater (Sanka, Rwiza, and Mtei 2020a).

1.4. Problem statement

Addressing industrial wastewater treatment is an urgent societal dilemma, highlighting the vital need for increased awareness to successfully manage the worldwide issue of water scarcity. The tannery business contributes significantly to water pollution by releasing harmful elements such as chemicals, residual colors, heavy metals, surfactants, salts, and chlorinated compounds. Despite its importance to worldwide industrial processes and economic growth, the industry offers environmental problems, notably as one of the greatest water users, with specific concerns regarding heavy metal pollution. Heavy metal pollution, particularly from Pb and Cr ions, poses a considerable risk to the environment due to their toxicity. Pakistan, ranking as the world's tenth largest rice producer, contributes over 8% to the global rice trade through its exports. Covering 3.15M hectares, or 11.7% of cultivated land, with an annual production of 11.12M tons in 2021-2022, 1M tons of rice yields 200K tons of rice husks (Memon et al. 2021). Furthermore, according to recent research, Pakistan cultivates bananas on over 35K hectares, yielding an average output of 4 tons per hectare and a total production of 154.8K tons. This production generates 43K tons of banana waste. In terms of area (93%) and production (83%), Sindh province leads, followed by Punjab, Khyber Pakhtunkhwa (KPK), and Baluchistan (Saeed et al. 2021). Despite their economic importance, conventional rice husk and banana peel

combustion and waste disposal practices pose environmental and health hazards and contribute to the existing waste management challenges. This emphasizes the urgent need for the regions in Pakistan where bananas and rice husks are prevalent to adopt sustainable waste management practices. Adsorption, one of the established conventional methods for removing heavy metals, is a cost-effective and ecologically beneficial wastewater treatment option. The applicability of biochar derived from both waste makes it a valuable product that can be used as an adsorbent to remove heavy metals from industrial wastewater. This is attributed to its porous structure, high surface reactivity, cost-effectiveness, enhanced carbon content, surface area and broad availability. This study focused on assessing the effectiveness of MgO impregnated biochar made from the co-pyrolysis of crop residue (rice husk) and fruit residue (banana peel) in simultaneously removing chromium and lead from synthetic wastewater.

1.5. Research objectives

The following are the objectives of this research:

1) Synthesis and characterization of Magnesium oxide (MgO) impregnated biochar made from co-pyrolysis of rice husks and banana peels.
2) Investigating the adsorptive exclusion potential of synthesized biochar for lead and chromium under single and binary system.

LITERATURE REVIEW

2.1. Removal methods of Lead and Chromium

Many treatment techniques, such as bioremediation (Kaur and Roy 2021a) (Ayele and Godeto 2021), electroplating (Ayub et al. 2020), ion exchange (Pan and An 2019), membrane separation (Yurekli 2016), adsorption (Alalwan, Kadhom, and Alminshid 2020), chemical precipitation (Benalia et al. 2022), flotation (Hoseinian et al. 2023), photocatalysis (Gao and Meng 2021) and coagulation flocculation (Sun et al. 2020) were utilized to eliminate metal ions from wastewater. Nanotechnology, alongside traditional methods, is rapidly being used to eliminate heavy metal ions from polluted water bodies (Kaur et al. 2021b). Due to the numerous drawbacks associated with the treatment options, there is a need for the development of an effective method. Such obstacles include significant sludge production in coagulation and flocculation and the generation of hazardous secondary solid waste in chemical precipitation, which requires additional disposal treatment. Membrane separation poses challenges such as cost, aging, regeneration difficulties, and rejection. Advanced oxidation processes are expensive and require complicated chemistry. Furthermore, controlling higher metal ion concentrations and disposing of foams are key hurdles for the flotation process. Ion exchange techniques lack the ability to recycle resin, which adds to their limitations (P. S. Kumar, Gayathri, and Rathi 2021a). Adsorption is the preferred method in wastewater treatment due to its effectiveness, avoiding drawbacks like sludge generation, low treatment quality, mild operating conditions, and expensive disposal associated with alternative approaches (Rajendran et al. 2022). Adsorbent selection for industrial wastewater is critical, as common adsorbents are sometimes unable to completely minimize concentrations to levels that are acceptable. The selection procedure needs to take metal ion types into consideration (Foroutan et al. 2022). The response surface design provided the best results for banana peels for lead (Pb) at an initial concentration of 100 mg/L, a pH of 5, an adsorbent dose of 0.55 g, and a particle size of 75 µm, resulting in a removal rate of 98.146% (Afolabi, Musonge, and Bakare 2021). Likewise, rice husk, a material high in inert silicon, serves as an excellent foundation for biochar production. According to research conducted in 2020, the best removal efficiencies for Cr (65%), Fe (90%), and Pb (>90%) were obtained by carbonizing rice husks at 600°C (Sanka, Rwiza, and Mtei 2020a). However, unmodified rice husk biochar's (RHB) adsorption efficiency is often unsatisfactory (A. Li et al. 2022). The combined pyrolysis (co-pyrolysis) of

different organic wastes has been proven to improve process performance (Karaeva et al. 2022). Magnesium oxide (MgO), with its high specific surface energy and easy doping properties, might also be a great inhibitor of biochar (A. Y. Li et al. 2020). The outstanding physicochemical properties of the original biochar enhanced with MgO make it a highly effective adsorbent for removing heavy metals from wastewater (Cheng et al. 2022a). (Ling et al. 2017) developed MgO@N-biochar to remove lead from wastewater with an adsorption capacity of 893 mg/g. Therefore, MgO-modified co-pyrolyzed biochar produced from banana peels and rice husks could simultaneously and effectively eliminate lead (Pb) and chromium (Cr) from wastewater. There are several techniques to remove heavy metals, particularly lead and chromium. Common techniques for eliminating these metals are:

➢ Chemical precipitation
➢ Coagulation-flocculation
➢ Electroplating
➢ Ion exchange
➢ Membrane treatment
➢ Adsorption

2.1.1. Membrane treatment

Membrane separation is a technique involving the passage of feed water via a semi-permeable membrane under high pressure to selectively detach substances from the solution. This technique encompasses microfiltration (MF), ultrafiltration (UF), nanofiltration (NF), and reverse osmosis (RO) based on pore size. The molecules or ions diffusion into the membrane depends on various factors such as solute concentration, membrane permeability, pressure and temperature. Three fundamental principles include electrostatic phenomena, adsorption and sieving direct this process. Adsorption occurs through hydrophobic interactions between the membrane and solute. Moreover, substance detachment depends on the membrane pore and solute size. Various membrane-based separation processes, using different mechanisms have been developed relies on these principles (Shrestha et al. 2021a). However, membrane filtration efficiently removes heavy metals from industrial effluents, its high cost, particularly for processing broad volumes of wastewater, creates a challenge. The membranes reverse cleaning is a complicated process which could lead to secondary contamination, restricting its practicality. The relationship between the pore size of membrane and solute size plays an

important role in finding how materials are detached in membrane-based processes (Y. Zhang and Duan 2020).

2.1.3. Chemical precipitation

Chemical precipitation removes ionic elements from wastewater by converting soluble compounds into insoluble forms. However, metal ions often precipitated as hydroxides or through sulphide and carbonate precipitation (Shrestha et al. 2021a). Chemical precipitation has several advantages, serving as an effective and straightforward method for treating heavy metal effluent. Traditionally, strong alkaline reagents such as ammonia, lime, sodium hydroxide, sodium carbonate, and sodium sulfide are used to elevate the pH of wastewater, causing heavy metal ions to precipitate in their insoluble forms (hydroxide, carbonate, or sulfide). However, conventional reagents have drawbacks, including the production of toxic hydrogen sulfide gas by heavy metal ions in acidic solutions, challenging filtration of small particle-sized heavy metal sulfides, and the formation of water-soluble coordination compounds by amphoteric metals like copper and chromium at pH levels exceeding the optimum range (Y. Zhang and Duan 2020). Furthermore, the chemical precipitation process generates significant amounts of sludge, necessitating treatment and disposal. The disposal of waste sludge with excessive salt concentrations poses environmental challenges as it fails to meet standards (P. S. Kumar, Gayathri, and Rathi 2021b).

2.1.4. Ion exchange method

Ion exchange is a water treatment process that removes one or more undesired ionic impurities from water by exchanging them with another non-objectionable, or less objectionable, ionic material. A common example of ion exchange is the "water softening" process, which aims to lower calcium and magnesium levels. However, ion exchange is effective in removing harmful metals from water. Moreover, this technique efficiently removes heavy metals that are mixed in water (P. S. Kumar, Gayathri, and Rathi 2021b). Based on their strong attraction to dissolved ions, primarily heavy metals, ion exchange resins prove highly efficient in purifying wastewater to fulfill stringent environmental discharge regulations (Ma et al. 2019). Extensive examinations over the past twenty years have highlighted notable benefits, including the method's capacity to eradicate concentrations of heavy metal at parts per billion (PPB) levels in large amounts and its efficacy in selectively purifying either cations or anions (Shrestha et al. 2021a). However, when dealing with concentrated metal solutions, the exchange matrix is vulnerable to sudden fouling by organic compounds and other solid components in the waste stream.

2.1.5. Coagulation and flocculation

Pollutants, contaminants, and suspended particles are effectively removed from water and wastewater via coagulation as well as flocculation. This affordable technique involves electrostatic repulsion by using coagulants to accelerate collisions and remove negatively charged particles. The coagulation process consists of three steps: coagulant addition, particle instability, and agglomeration, which require the addition of chemicals and temperature regulation. Coagulants include synthetic polyelectrolytes, organic polymers, and inorganic electrolytes like aluminium and iron complexes. Flocculation, that includes adding high-molecular-weight polymers to make the small particles adhere to one another, is another method of eradicating waste pollutants. Small flocs are produced as a result, which facilitate their ultimate removal by filtering or sedimentation. Anything from hydrated lime and magnesium carbonates to iron and aluminium compounds might be a coagulant. Collectively, flocculation and coagulation provide a capable and effective strategy. When combined with other traditional techniques, coagulation-flocculation can be used to remove metal pollution from wastewater (Saleh, Mustaqeem, and Khaled 2022).

2.1.6. Electrochemical process

This technique transfers metal ions and direct current between insoluble anode and cathode plates via an aqueous solution. Where, the negatively charged electrode attracts positively charged ion and deposition takes place at the cathode (Shrestha et al. 2021b). However, its constant current supply requirement makes it costly, limiting its use in countries with high electricity costs. Many prefer traditional filtration methods due to these challenges. Conventional electrochemical treatments, such as electrocoagulation, electrodeposition, electro disinfection, electrooxidation, and electro flotation (Saleh, Mustaqeem, and Khaled 2022), offer alternatives. Despite the cost challenges, electrochemical processes provide benefits like metal selectivity, no extra reagent needs, fast removal, and reduced sludge production. However, this process has limitations, including pH sensitivity, frequent electrode replacement, and high energy and electrode costs (Raouf and Raheim 2016).

2.1.6.1. Electrocoagulation

Electrocoagulation utilizes electrical current to efficiently remove metals, suspended particles, dissolved metals, tannins, and pigments from a solution. Electrical charges keep contaminants in wastewater, neutralizing particles and forcing them to precipitate in a stable state. This electrochemical approach is efficient, cost-effective, user-friendly, and ecologically friendly, generating potable, clear, colorless, and odorless water with minimum sludge development,

thereby preventing future water pollution. Electrocoagulation's versatility makes it an attractive choice for treating a wide range of industrial wastewaters, such as landfill leachate, restaurant, carwash, butcher, textile, laundry, tannery, and petroleum refinery wastewater. Furthermore, it successfully eliminates bacteria, arsenic, fluoride, pesticides, and heavy metals from water (Bazrafshan et al. 2015). Despite its benefits, electrocoagulation has several drawbacks as well, including electrode passivation, increased energy consumption due to poorer wastewater conductivity, and the possibility of secondary contaminants in compounded wastewater conditions (Akter, Suhan, and Islam 2022).

2.1.7. Adsorption

Adsorption is a surface phenomenon that is characterized by a specific substance adhering to a solid object's surface through chemical bonds or physical forces (Pandey et al. 2021). Pollutants, commonly referred to as adsorbates, stick to a solid surface called an adsorbent by the process of adsorption. The three main stages of the adsorption process include transport within the adsorbent particle, on the particle surface, and adsorption of solutes onto the adsorbent surface. However, the rate of adsorption is influenced by several factors, such as temperature, the nature of adsorbent and adsorbate, interfering contaminants, and ambient parameters such as pH, concentration and contact time). Several adsorbents have been studied, including activated carbon, graphene oxide, rice husk, sugarcane bagasse, wheat bran, coconut waste, orange peel, sawdust, eggshell, mesoporous silica, chitosan, zeolite, red mud, powdered olive stones, apple pomace, alumina, clay, fungal biomass, and algal biomass (Thomas, Lai, and Bin Johan 2019;Sepehri Sarrafzadeh, Avateffazeli 2020, and Singh et al. 2018). Activated carbon has been a popular choice for treating and recycling wastewater since the 1940s. Due to its small particle size, numerous active sites and large surface area, it is a highly effective adsorbent. However, the high manufacturing and regeneration costs of activated carbon make it unsuitable for large-scale water treatment applications (Shrestha et al. 2021a). Therefore, it is crucial to identify novel, affordable, and efficient adsorbents for the remediation of aquatic systems contaminated by heavy metals. Researchers are attracted to these inexpensive adsorption technologies because they are effective at eliminating heavy metal ions from solute systems. Compared to activated carbon, other biomasses offer advantages such as easier disposal, superior adsorption capacity, regeneration capabilities, and the ability to recover and reuse metals (P. S. Kumar, Gayathri, and Rathi 2021b). Biochar, an economically feasible adsorbent with simple ion exchange, stability and good performance (Lee and Shin 2021), is a carbon-rich substance produced by heating byproducts at high temperature in the absence of

oxygen (Ni et al. 2019). Its numerous micro- and nanopores, together with functional groups like hydroxyl and carboxyl, are responsible for its remarkable tendency to hold pollutants, including heavy metals (T. Wang et al. 2018). In aquatic environments, raw and unmodified biochars have long equilibrium durations and limited adsorption potential. To enhance pollutant adsorption, engineered biochars are preferred (Lakshmi et al. 2021). However, biochar's potential for heavy metal removal is limited by its low adsorption and cycling performance, demanding novel ways for creating efficient absorbents incorporating biochar as a basic material (A. Li et al. 2022). Banana peels provide an excellent source of activated carbon due to the presence of cellulose and hemicellulose. The peel's surface contains hydroxyl, carboxyl, and amide groups, which enable them to remove heavy metals (Ying tao Sun et al. 2023). Improper management of tons of banana peels generated daily leads to odor issues and the release of greenhouse gases. The surface of banana peels features a diverse array of functional groups, including carboxyl, amide, hydroxyl, phenolic, and methoxy groups, which collectively contribute to its exceptional biosorption capabilities (Oladipo, Ahaka, and Gazi 2019a). Kadirvelu et al. discovered that coir pith carbon effectively removed 73% of Cu (II), 100% of Hg (II), Pb (II), and Cd (II), and 92% of Ni (II) (Kadirvelu et al. 2001). (Saleh and Ali 2018; Saleh et al. 2020) invented a simple reversible desorption method for renewing adsorbent. This approach successfully eliminates pollutants at low concentrations requires no further waste management and generates little sludge. This method is easy to apply and affordable (Saleh and Ali 2018; Saleh et al. 2020). The efficiency of several adsorbents in eradicating heavy metal ions from aqueous solutions were examined in a research study conducted in 2014. These adsorbents covered biochar derived from rice husk, the organic content of municipal solid wastes, sewage sludge and sandy loam soil. For initial Cr (III), the materials under investigation showed a removal efficacy above 95%. As (V) and Cr (VI) anions, however, had significantly reduced removal rates. Sewage sludge-derived biochar showed effective removal, with 89% removal efficiency (Agrafioti, Kalderis, and Diamadopoulos 2014). Another comprehensive study was conducted in 2023 by Waleed Usmani to contrast the effectiveness of Mg-Fe LDH@OPP composite and raw orange peel powder (OPP) in removing Cr (VI) ions from synthetic aqueous solution. Its sorption capacity increased due to its bigger particle size, greater point of zero charge, and large surface area, increased. (Usmani et al. 2023). Cotton stalk biochar (CSB) generated at different pyrolysis temperatures, demonstrated efficient hexavalent chromium (Cr (VI)) removal from water. Despite CSB500 having the lowest surface area, it exhibited superior adsorption performance under optimized conditions (pH 2, contact time of 2 hours, and biochar dosage of 3 g/L),

attributed to electrostatic attraction, Cr (VI) reduction to Cr (III), and complexation. The study provides valuable mechanistic insights into the environmentally friendly use of biochar for Cr (VI) species removal in aquatic environments, offering potential applications for a wide range of environmental scholars (Khalid and Inam 2024). Agricultural waste, i.e., rice husks, is very good at adsorbing metals, particularly zinc, from wastewater. The adsorption follows the Langmuir isotherm model, with a maximum capacity of 0.3 mmol/g for zinc and 0.003 mmol/g for lead. It is controlled by pH, rice husk dose, and contact duration. The study demonstrates the potential of rice husks in treating zinc and lead-contaminated wastewater by revealing a significant reduction in Zn^{2+} and Pb^{2+} concentrations in dairy effluent, with maximum removal percentages of 70% for zinc and 96.8% for lead (Asrari, Tavallali, and Hagshenas 2010). Another relevant study investigated the adsorption of metals (Cu^{2+}, Zn^{2+}, Co^{2+}, Ni^{2+}, and Pb^{2+}) from synthetic solutions using banana and orange peels treated with acid, alkali, and water. Both peels exhibited favorable adsorption, with banana peel showing Pb (II) ions sorption capacity of 7.97 mg/g and orange peel reaching 7.75 mg/g. Overall, the results suggest the potential utility of banana and orange peels in efficiently removing trace metals from synthetic solutions (Annadurai, Juang, and Lee 2002).

2.1.7.1. Types of Adsorbents
2.1.7.1.1. Nano Adsorbents

Many studies seek to create effective and affordable nano-adsorbents for eliminating heavy metal ions from effluents. Some well-investigated adsorbents include graphene, nano sized metal oxides, carbon nanotubes, and zeolite. The removal effectiveness of these adsorbents has been modified by their form, size, physical, and chemical properties. Zeolites are ideal for removing heavy metals from wastewater due to their large surface area, hydrophilic nature, and excellent ion exchange characteristics. The most common natural zeolites such as analcime, chabazite, clinoptilolite, erionite, faujasite, ferrierite, laumontite, mordenite, and phillipsite are found in volcanic rock (Burakov et al. 2018). Carbon nanotubes (CNTs) were first identified in 1991 (Iijima). Carbon cylinders can be single or multi-walled, shaped like rolled graphite sheets, with diameters ranging from one-to-many tens of nanometers and lengths of several centimeters. CNTs have opened new research opportunities because of their unique structural, electronic, optoelectronic, semiconductor, mechanical, chemical, and physical capabilities (Haddon 2002; Burakov et al. 2018). Graphene, discovered in 2004, is a two-dimensional hexagonal lattice composed of carbon atoms. It, like CNTs, has distinct structural, mechanical, physical, and chemical characteristics that make it suitable for use in a variety of applications. Microwave-synthesized carbon nanotubes showed great performance as adsorbents for Pb^{2+}

and Cr^{3+} removal from wastewater, with optimal conditions at pH 4.0 and pH 8.0, respectively. The study found remarkable removal efficiencies of 99.9% for Pb^{2+} and 95.5% for Cr^{3+}, with maximum capacities of 15.34 mg/g and 24.45 mg/g, respectively (Mubarak et al. 2016). Graphene exists in multiple forms, such as pristine graphene, graphene oxide (GO), and reduced graphene oxide (rGO). Their unique properties, including their high specific surface area, abundant active sites, diverse functional groups, and exceptional chemical stability, make them highly sought after for environmental remediation, particularly in industrial effluent applications (Gopalakrishnan et al. 2015). At an initial dosage of 50 mg/L, the magnetic chitosan graphene oxide (MCGO) composite material reveals remarkable efficiency, removing 92% of Pb (II) ions in 420 minutes at pH 5, 27°C. Moreover, favourable thermodynamics also suggest that it could serve as a reusable and efficient adsorbent (Samuel et al. 2018). Titanium dioxide (TiO_2), iron oxide (Fe_2O_3), zinc oxide (ZnO), aluminum oxide (Al_2O_3), magnesium oxide (MgO), cerium oxide (CeO_2), copper oxide (CuO), manganese oxide (MnO_2), nickel oxide (NiO), and silver oxide (Ag_2O) are among the metal oxide nano adsorbents that are used for their efficient adsorption capabilities in a variety of applications. Nano-sized metal oxides (NMOs) are a preferred adsorbent material because of their remarkable adsorption capacity, flexibility in synthesis and modification, affordability, and mass production scalability. Their distinct ability to remove contaminants at trace levels, even at low concentrations, is a significant benefit over conventional adsorption techniques (Wang et al. 2020). The study confirmed the efficient removal of Cr (VI) utilizing nano-sized metal oxides (CuO, NiO, SnO, SnO_2, Zn_2SiO_4) by batch adsorption in real-world applications for industrial and drinking water samples. High removal efficiency of 99.3% and 88.6% were observed by NiO and SnO nanoparticles, respectively. The techno-economic analysis estimated that the average cost of the produced nanometal oxides would be 2.3 USD per gram (Masoud et al. 2023).

2.1.7.1.2. Biosorbents

Another highly effective wastewater treatment method known as bioremediation, or biosorption, is renowned for its capacity to remove heavy metal ions from effluents and for having cost-effective expenses for operations. Biosorbents, which include a variety of biomaterials such as bacteria, algae, agricultural waste and industrial waste, are acknowledged for being renewable, affordable and biodegradable, with no secondary pollutants generated after usage. Multiple functional groups in biosorbents, which are derived from biological sources, drive their hydrophobic contact in a sorption process which is pH dependent. Utilizing the synthesis of biomass, especially from fungi and bacteria, turns out to be more economical

than using conventional resources. Known for their non-toxic and renewable biomass, algae have become more popular for their capacity to accumulate a significant quantity of metals. Moreover, its abundance in the marine environment lowers processing costs. Microalgae are essential to wastewater bioremediation as they are skilled at breaking down nutrients (Adewuyi 2020; Chai et al. 2021). Ludwigia stolonifera, a natural biosorbent generated from roots and shoots, was successful in removing Pb^{2+} (81.4%) and Cr^{6+} (77%) from aqueous solutions (Amier et al. 2021).

2.1.7.1.3. Agricultural Byproducts

The natural environment contains huge quantity of agricultural waste and its byproducts. Lignin and cellulose are the two dominant constituents of agricultural waste. Cellulose is a crystalline homopolymer containing β1-4-linked glucosyl units. Moreover, agricultural residues contain different components such as ash, proteins, carbohydrates, simple sugars, lipids, and hemicellulose. Agricultural derived adsorbents, comprising materials such as fruit and vegetable peels, wheat straw, sawdust, rice husk, tea waste, nutshell, and plant residues, contain selective affinity for metal ions based on their unique compositional characteristics (P. S. Kumar, Gayathri, and Rathi 2021a). The fruit sector causes a major environmental issue since it creates a large amount of waste, which takes part in pollution. Anaerobic waste degradation in fruit disposal emits undesirable odors and harmful gases, negatively impacting the atmosphere and diminishing the concentration of natural gases. The banana chip manufacturing sector grapples with a significant issue in managing banana peel waste, resorting to various landfilling procedures. However, researchers have sought innovative solutions to address this problem by transforming banana peels into value-added products. Instead of discarding banana peel trash, researchers have successfully recycled it to remediate heavy metal-contaminated water. This not only reduces environmental impact, but it also helps the businesses involved financially (Van Thuan et al. 2017; D. Yu, Wang; Wu 2018; Rani et al. 2019, and Saleem and Saeed 2020). Annually, the world produces roughly 80 million tons of rice husk, accounting for approximately 23% of the residual output from every ton of processed rice. Notably, it serves as a precursor for adsorbents, leveraging its chemical stability, and insolubility in water, cost-effectiveness, granular form and readily available locally. Despite its diverse uses, the open firing of rice husks poses environmental challenges, releasing carbon dioxide and other hazardous chemicals into the atmosphere, thereby contributing to pollution. The composition of rice husks varies based on geographical location, climate, soil qualities, fertilizer type, rice classification, and paddies. Comprising cellulose, hemicellulose, lignin, ash,

water, and extractives, rice husks contain carbon and silica, functioning as effective adsorbents for removing hazardous contaminants from wastewater (Nath, Chaliha, and Kalita 2019; Mahmoud, Fekry, and Abdelfattah 2020; Khalil et al. 2020). The study investigated the efficacy of solid waste materials in removing trivalent chromium (III) from tannery wastewater. Among agricultural wastes (rice husk, rice straw, sugarcane bagasse, sawdust) and industrial wastes (cement kiln bypass dust, marble powder), cement kiln dust and marble powder exhibited the highest chromium removal, surpassing 99% efficiency when the solution's pH exceeded 8.75 (Abdelkader et al. 2021). The adsorption capabilities of modified biochar (MBCW600), which is generated from crofton weed and increased with MgO, are higher than those of original biochar for Pb^{2+} (384.08 mg/g) and Cd^{2+} (207.02 mg/g) in wastewater. The investigation demonstrates effective removal approaches mainly by precipitation and ion exchange, which makes MBCW600 a material with notable adsorption capability that shows potential for use in the treatment of heavy metal wastewater (Cheng et al. 2022b). Another relevant study utilized biochar made from rice husk, wheat straw, and corncob as an ecologically acceptable adsorbent for heavy metal removal. These biochar's have high lead (Pb^{+2}) adsorption capacities of 96.41%, 95.38%, and 96.92%, as well as cadmium (Cd^{+2}) absorption capabilities of 94.73%, 93.68%, and 95.78%, making them viable options for cleaner water production (Amen et al. 2020). During this investigation, rice husk powder treated with 0.1 N HCl showed efficient adsorption of chromium (87.12%), lead (88.63%), and zinc (99.28%) from aqueous solutions. The optimal conditions were a pH of 6.0, a contact period of one hour, a rice husk dose of 2.5 g/L, and a temperature of 30°C, demonstrating its promise as a low-cost biosorbent for heavy metal removal from industrial effluents (Priya et al. 2022a).

MATERIAL AND METHODS

3.1. Materials and Chemicals

Banana peels and rice husks were obtained from a market in Punjab, Pakistan. Reagent-grade chemicals have been purchased from Sigma Aldrich (USA) included iron sulphate ($FeSO_4$), magnesium chloride hexahydrate ($MgCl_2.6H_2O$), acetone, potassium dichromate ($K_2Cr_2O_7$), 1,5-diphenylcarbazide, lead nitrate ($PbNO_3$), hydrochloric acid (HCl), sodium hydroxide (NaOH), orthophosphoric acid (H_3PO_4), ammonium chloride (NH_4Cl), glucose ($C_6H_{12}O_6$) and potassium dihydrogen phosphate (KH_2PO_4).

3.2. Preprocessing of materials

The banana peels were washed with tap water, then distilled water, then dried for a day at 80°C (Foroutan et al. 2022). The rice husks were first manually cleaned before being boiled in deionized water for 5 hours to remove the color. The husks were filtered and dried for 24 hours at 80°C in a hot air oven (Tariq et al. 2019). Furthermore, dried rice husks and banana peels were crushed into powder, sieved through No. 20 mesh (0.841 mm). The powder was kept in zip-lock bags and stored in the desiccator.

3.3. Synthesis of raw biochar

Through pyrolysis, three kinds of unmodified, or raw, biochar (RBC) were generated: 1) RHBC, or rice husk biochar 2) Biochar made from banana peels (BPBC) 3. CBC, or combined biochar. This was completed by adding rice husk powder, banana peel powder, and a mixture of the two powders in an equal (1:1) ratio into a pyrolysis reactor set up in a nitrogen atmosphere at 550°C for three hours at a flow rate of 0.2 L/min. Prior to and following the experiment, nitrogen purging was carried out for 20 minutes at a rate of 0.5 L/min. Further, all three forms of raw biochar were kept in Ziplock bags after being passed through a mesh size of 325 (0.04 mm) (Irfan et al. 2023). Table 1 shows the yield of biochar, biogas, and bio-oil that resulted during the pyrolysis process. The yield of the final product (biochar) was determined using Eq. 1, depending on the mass of the sample inserted into the reactor.

$$Y(\%) = \frac{x}{x'} \times 100 \qquad (1)$$

Where, x is the mass, in grams, of the biochar and x' is the mass, in grams, of the sample. Among the biomasses examined, the RHP: BPP mixture exhibited a lower biochar yield of 39% compared to RHP (40.56%) and BPP (42.78%). The yield of pyrolysis and a schematic of the pyrolysis reactor are provided in table 3.1 and fig. 3.1, respectively.

Table 3.1: Yield of Pyrolysis

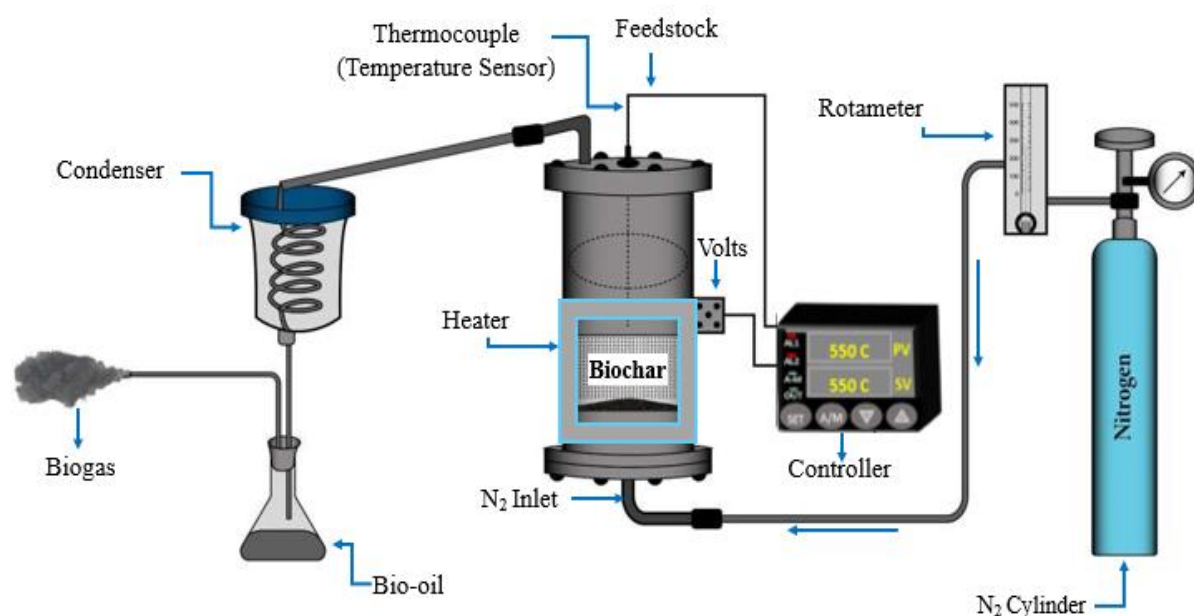| Sr. No.	Type of Materials	Percentage Yield (%)		
		Biochar	Bio oil	Biogas
1	Rice husk powder	40.56	9.66	24.89
2	Banana peel powder	42.78	20.44	36.78
3	Combined Powder	38.6	12	49

Figure 3.1: Schematic of pyrolysis reactor

3.4. MgO modification of biochar

For activation, 30 grams of biochar (BC) were mixed with 40.66 grams of $MgCl_2 \cdot 6H_2O$ in 200 mL of distilled water, and the mixture was stirred for 24 hours. Following this, the mixture was dried in a hot air oven at 80°C for 24 hours. The resulting dried powder was then transferred into a pyrolysis reactor, and nitrogen purging was applied at a rate of 0.5 L/min for 20 minutes before starting the experiment. Subsequently, the mixture was then heated in a reactor at a temperature of 400°C for 60 minutes under a nitrogen atmosphere (0.2 L/min) to ensure an oxygen-free environment. Upon completion of the experiment, nitrogen purging was again carried out for twenty minutes at flow rate of 0.5 ml/min. Biochar powder obtained from this preparation process was identified as MgO-modified biochar (Cheng et al. 2022b).

3.5. Preparation of stock solutions

Stock solution of 1000-ppm Cr (VI) was obtained by adding 0.285 g of potassium dichromate in 100 mL of distilled water. Further, a 100-ppm dilute solution was prepared by mixing 10 mL of the stock solution with 90 mL of distilled water. Working solutions formed by adding suitable quantities of the dilute solution to distilled water. A 1000 (ppm) stock solution of Pb (II) was obtained by adding 0.1616 g of lead nitrate in 100 mL of distilled water. For a concentration of 100 (ppm), 0.01616 g of lead nitrate dissolved in 100 mL of distilled water. Intermediate solutions produced by combining estimated quantities of the stock solution with distilled water. Intermediate working solutions with the required concentrations were prepared using 1000 and 100 ppm stock as well as diluted solutions of both Cr (VI) and Pb (II) in the case of combined synthetic wastewater. The formula used for these intermediate solutions is $M_1V_1 = M_2V_2$, where M1 represents the initial concentration, V_1 denotes the initial volume, M_2 signifies the required concentration, and V_2 represents the total final volume. When dealing with dilute aqueous solutions, V_2 represents the sum of the volumes that were mixed.

To adjust the pH as needed, solutions of 0.1 molar HCl and 0.1 molar NaOH were synthesized. For 0.1 molar hydrochloric acid, 0.83 ml of pure HCl was added with 99.17 ml of distilled water, and for 0.1 molar sodium hydroxide, 4 g of NaOH was added with 100 ml of distilled water. Prior to conducting the adsorption tests, all glassware and containers used for samples were to be thoroughly washed with a 15% HNO_3 solution and then rinsed with distilled water.

3.6. Batch Adsorption
3.6.1. Experimental design and conditions

A series of batch adsorption experiments were carried out using 250-mL conical flasks to assess the individual and combined removal capabilities of lead and chromium from simulated wastewater representative of tannery industry effluent. Initially, we examined the effects of different doses of RBC and MgO@BC (1, 2, 4 g/L) using 100 mL of synthetic chromium solution, lead solution, and a combined solution at pH 2 and 4. The solutions were stirred for 2 hours at 180 RPM. Isotherm studies were conducted by varying the initial concentrations of lead and chromium in separate synthetic wastewater samples as well as in a combined synthetic wastewater sample (ranging from 10 to 100 mg/L, i.e., 10, 20, 40, 60, 80, and 100). These experiments were carried out under solution conditions of pH 2 and 4, with a contact time of 2 hours and a constant dosage of 2 g/L MgO@CBC. These experiments were conducted using an orbital shaker. Following the adsorption experiments, all samples underwent filtration using

Nylon-cellulose membrane filter (0.22 μm). Reagent solution for chromium was obtained by dissolving 0.5 g 1,5-diphenylcarbazide in 100 mL acetone. For lead analysis a 0.195 molar dithizone reagent solution was obtained by dissolving 0.00495 g dithizone using 100 mL of distilled water. Additionally, a 0.3 molar CTAB (Cetyltrimethylammonium Bromide) solution was prepared by dissolving 10.93 g of CTAB in 100 mL of distilled water. Furthermore, a 0.004 molar HCl solution was prepared by diluting 0.03 millilitre of concentrated HCl in 100 mL of distilled water. UV SPECORD 200, Analytik Jena, was utilised to detect the filtrates of Pb and Cr at specific wavelengths: 500 nm for Pb and 540 nm for Cr (Usmani et al. 2023). The concentrations of both chromium and lead were determined, and removal efficiencies along with adsorption capacities were computed using Eq. 2 and 3, respectively. The equations are as follows:

$$R = \frac{(Co-Ce)}{Co} \times 100 \tag{2}$$

$$q_e = \frac{(Co-Ce)V}{m} \tag{3}$$

Ce and Co are the initial and final metal concentrations (mg/L), m is the mass of the adsorbent (g) and V is the volume (L).

3.6.2. Chromium calibration curve

To establish the calibration curve for Cr (VI) concentration ranging from 0.1 to 2 mg/L, the following procedure was followed:

- First, a 1000 ppm Cr (VI) stock solution was prepared. Next, it was diluted to 100 ppm. Took 0.1, 0.2, 0.5, 1, 1.5, and 2 ml from the previously prepared dilute solution. Transferred each volume into separate labelled volumetric flasks. Prepared a blank by taking 100 ml of distilled water in a flask. Added 3 to 4 drops of orthophosphoric acid. Waited for 5 to 10 minutes, then added 2 ml of the prepared reagent. Zeroed the spectrophotometer using the blank solution. Measured the absorbance of each sample at the 540 nm wavelength for chromium determination.

- Plotted a calibration curve with concentration (mg/L) on the x-axis and absorbance on the y-axis. Determined the equation of the line and coefficient (R^2) for the calibration curve.

- Used the calibration curve to determine the concentration of Cr (VI) in unknown samples by measuring their absorbance and interpolating from the calibration curve.

The coefficient of determination (R^2) for the curve was calculated as 0.9992. Details of the calibration curve data are provided in table 3.2, with a graphical representation shown in fig. 3.2 below:

Table 3.2: Cr (VI) standard calibration curve data

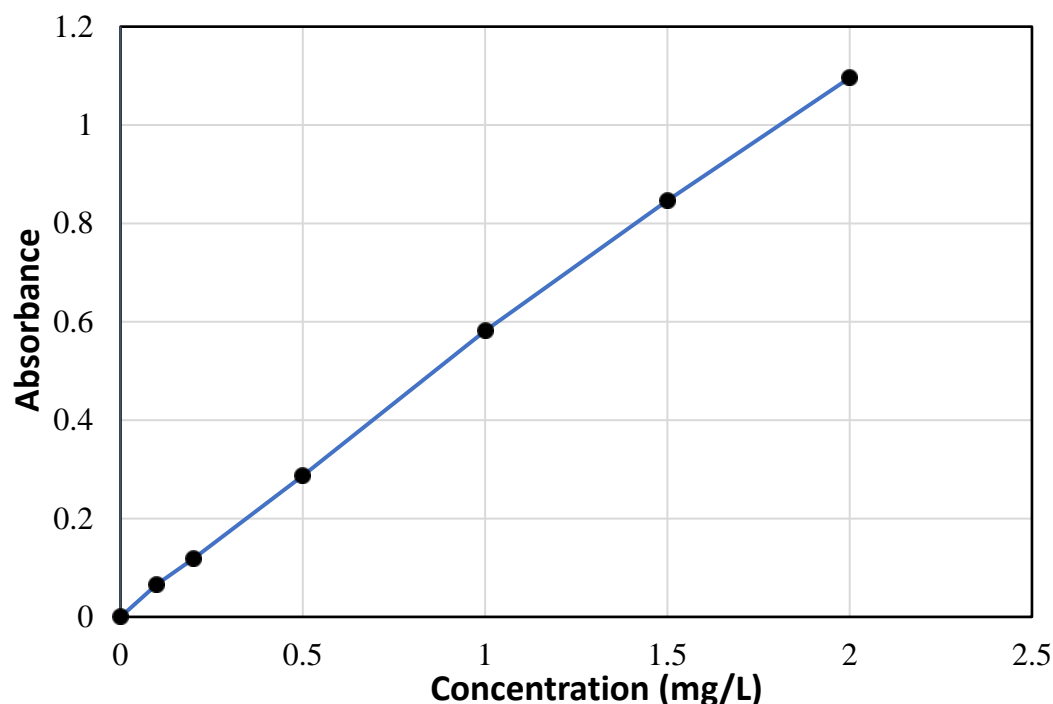| Concentration (mg/L)	0.0	0.1	0.2	0.5	1	1.5	2
Absorbance	0.0	0.0664	0.1186	0.2872	0.5816	0.8463	1.0959

Figure 3.2: Cr (VI) calibration curve

3.6.3. Lead calibration curve

A calibration curve for Pb (II) concentrations between 0.05 and 10 mg/L was established through the following steps:

- A 100-ppm stock solution of Lead (II) was prepared. Then, a series of lead solutions (100 mL each) with concentrations ranging from 0.05 to 10 mg/L were prepared by diluting the stock solution in a serial manner.
- A 10 mL analytical solution was prepared by mixing:
  - 3.5 mL of the lead solution, 1.5 mL of 0.195 M dithizone, 1 mL of 4 mM HCl, and 4 mL of 0.3 M CTAB
- A blank solution was prepared by replacing the lead solution with 3.5 mL of distilled water, while keeping the other reagents the same. The solutions were analyzed in a spectrophotometer at 500 nm wavelength. The calibration curve yielded a coefficient of

determination (R^2) of 0.953. Calibration curve data are detailed in table 3.3, with a corresponding graphical representation illustrated in fig. 3.3 below:

Table 3.3: Pb (II) standard calibration curve data

Concentration (mg/L)	0.05	0.3	0.4	0.5	0.9	1	3
Absorbance	0.1369	0.1376	0.1384	0.1383	0.1407	0.1404	0.145
Concentration (mg/L)	4	5	6	7	8	9	10
Absorbance	0.1501	0.1597	0.1609	0.1679	0.183	0.1844	0.1982
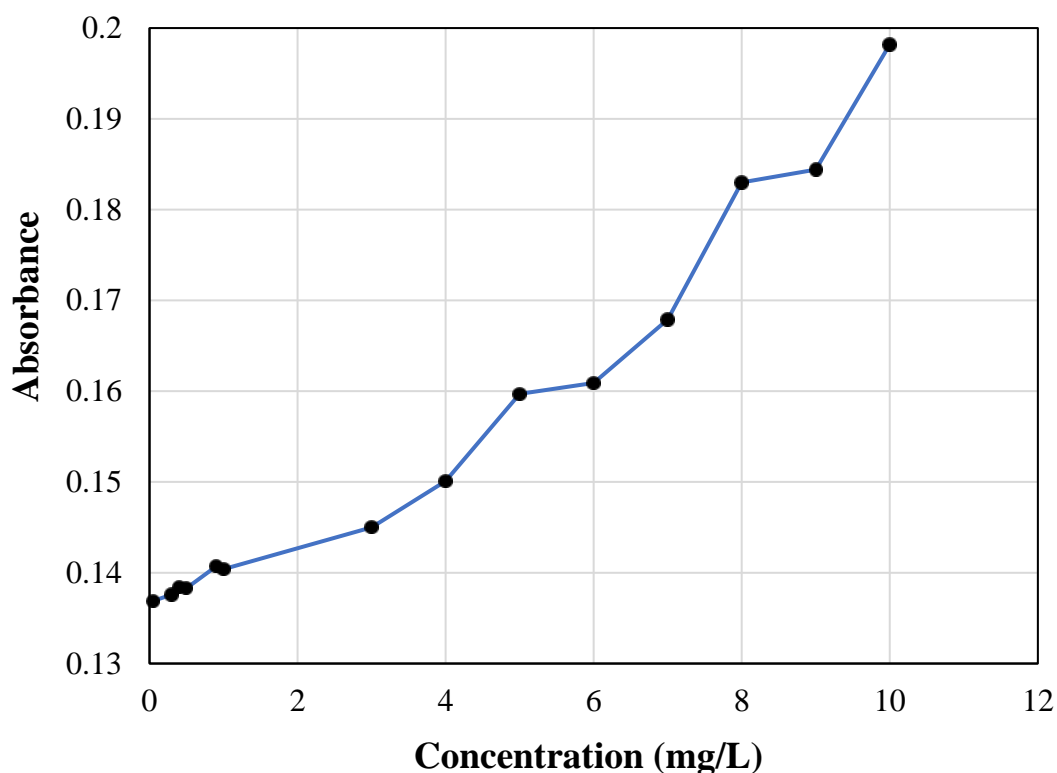
Figure 3.3: Pb (II) calibration curve

3.7. Proximate analysis

The proximate analysis of raw biomass powder, RBC, and MgO@BC was performed following ASTM standard methods (ASTM E871–82, E872-82, and D3175–11) for moisture analysis, volatile matter, and ash using an oven and muffle furnace. This analysis involves assessing the main constituents of a material, usually expressed as percentages of its total weight. Proximate analysis focuses on four key components:

- **Moisture Content:** This is the percentage of water present in a biomass sample when it is heated slightly above the boiling point of water (105°C) Eq. 4.

- **Volatile Matter:** Refers to the portion of a substance that evaporates when subjected to high temperatures, typically 950°C ± 20°C, in a muffle furnace. It can indicate how easily a material will burn Eq. 5.

- **Ash Content:** This is the residue left after a biomass sample is heated at 650°C ± 50°C, where moisture evaporates, and volatile matter burns off. The residue, known as ash, contains no energy and consists of inorganic materials Eq. 6.

- **Fixed Carbon:** It refers to the carbon content that remains after removing moisture, volatile matter, and ash from the biomass. This parameter is critical for understanding the carbon composition of the material Eq. 7.

$$\text{Moisture Content} = \frac{X1 - X2}{X1} \times 100 \tag{4}$$

Whereas x_1= Sample initial weight (before oven dry at 105^0C); x_2= Sample final weight (after oven dry at 105^0C)

$$\text{Volatile Matter} = \frac{X3 - X4}{X3} \times 100 \tag{5}$$

x_3=Final weight (moisture content); x_4= Sample final weight (after heating at 950^0C)

$$\text{Ash} = \frac{X4 - X5}{X3} \times 100 \tag{6}$$

x_5=Final weight of sample obtained (after heating at 650^0C)

Fixed Carbon=100-Volatile matter (VM)-Ash (7)

3.8. Point of zero charge

The pHpzc of all raw and modified biochar was determined using the potentiometric titration method (Bakatula et al. 2018; Irfan et al. 2023). In this method, 0.2 grams of biochar added to 40 mL of 0.1 molar sodium nitrate solution in 50 mL conical flasks. The initial pH (pHi) adjusted between 2 and 10 using 0.1 molar HCl and 0.1 molar NaOH solutions. The flasks placed on a platform shaker for 24 hours at 180 rpm. After 24 hours, each sample filtered, and the final pH (pHf) checked. The pHpzc found out by plotting ΔpH (= pHf – pHi) against pHi.

3.9. Isotherm models

The non-linear Langmuir (Eq. 8) and Freundlich (Eq. 9) isotherm models are given as:

$$qe = \frac{qmK_LCe}{1+KCe} \tag{8}$$

$$qe = K_FC_e^{(1/n)} \tag{9}$$

The variables used in the isotherm models are qe (mg/g), representing the equilibrium adsorption capacity denoting the maximum amount of Cr (VI) and Pb (II) species that can be adsorbed onto the surface sites of MgO@CBC at equilibrium.; Ce (mg/L), the equilibrium residual concentration; qm (mg/g), the maximum adsorption capacity; K_L (L/mg), a Langmuir constant indicative of adsorption energy; K_F, a Freundlich constant related to adsorption capacity; and n, a Freundlich exponent characterizing surface heterogeneity

3.10. Analytical procedures

Surface morphology and elemental composition were examined using an SEM-EDX analytical scanning electron microscope (JSM-6490A by JEOL, Japan). The functional groups of RBC, MgO@BC, and AR: MgO@BC (MgO@BC post Pb and Cr adsorption) were analysed via spectrum 100 FTIR Spectrometer (PerkinElmer by Singapore). X-ray diffraction analysis was carried out using the XRD Bruker D8 Advanced X-ray diffractometer (Bruker by Germany) to explain the crystallographic structure of RBC, MgO@BC, and AR: MgO@BC. The surface area, pore volume and pore size of the materials were measured by Brunauer-Emmett-Teller (BET) method with Micromeritics Instrument Corp. (micromeritics, USA).

3.11. Degree of crystallinity and crystallite size

The degree of crystallinity (DOC%) was calculated using Eq. 10:

$$Xc = \frac{Ac}{Ac+Aa} \tag{10}$$

Where Ac is the area under crystalline diffraction patterns and Aa is the area under amorphous diffraction patterns. Similarly, the crystalline size was calculated using the Debye-Scherrer Eq. 11 (Zhu et al. 2020a).

$$D = \frac{K\lambda}{\beta \cos\theta B} \tag{11}$$

Where D, K, λ, β, and θ_B represent crystallite size (nm), shape constant (K = 0.9), X-ray wavelength (λ = 0.15406 nm), peak width at half maximum height (radians), and reflection angle (radians), respectively.

<div align="right">**CHAPTER 4**</div>

RESULTS AND DISCUSSION

4.1. Characterization of RBCs and MgO@BCs
4.1.1. SEM-EDX Analysis

The surface morphology of RBCs and MgO@BCs composites has been investigated using SEM fig.4.1, and the chemical composition was ascertained using the EDX technique. RHBC revealed an agglomerated mass with angular, dense, and a rough surface with scattered flaky particle (Shafiq, Alazba, and Amin 2023; Saravanan et al., 2021). BPBC consists of non uniform clustered mass, resembling a polygonal structure, with a slightly rough surface, revealing the presence of small pores (Sun et al. 2023). The pores and surface irregularities observed in BPBC may be attributed to the generation of volatile compounds such as hydrocarbons, water, carbon monoxide, and carbon dioxide (Tang et al. 2019). Combined biochar (CBC) indicated linked sheets with a longitudinal architecture. This morphology may result from the fibrous nature of both byproducts (banana peels and rice husks) (Izhar et al. 2022) and the vascular structures of banana peels. The thermal degradation of organic materials during this process keeps these fibrous frameworks intact. However, high temperatures and chemical reactions may result in the development of elongated rods from degraded lignin and cellulose. MgO@RHBC surface observed honeycomb porous structures and multiple coalesced particles might assist deposition and MgO loading (Xiang et al. 2018a). MgO@BPBC presented an uneven distribution of magnesium oxide forming a porous lamellar structure featuring connected mesopores and macropores. Furthermore, this non-uniform, three-dimensional, spherical morphology with a rough and heterogeneous surface enhances adsorption capabilities (Yang et al. 2023). The surface of MgO@CBC exhibited a rough texture characterized by varying-sized particles, along with internally agglomerated and somewhat detached pores, while numerous particles were observed on the surface. Overall, the SEM photograph reveals that Mg@BC has a porous structure made of carbon flakes, while C, O, Mg, and Cl are irregularly distributed according to the EDX spectrum, confirming the successful synthesis of Mg@BC (A. Li, Ge, et al. 2022a). EDX analysis of RBCs and MgO@BCs is presented in table 4.1.
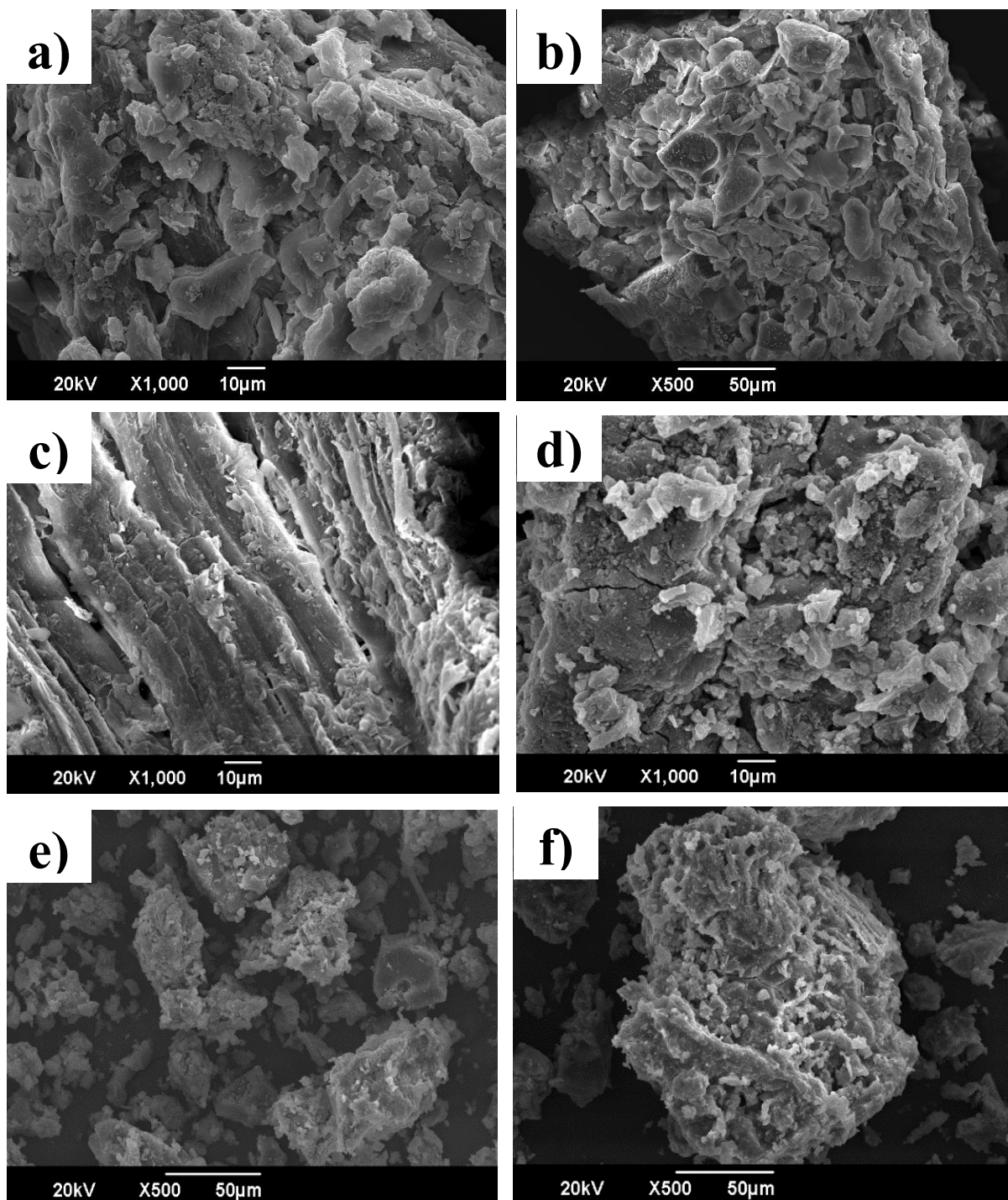
Figure 4.1: SEM Images

a) RHBC, b) BPBC, c) CBC, d) MgO@RHBC, e) MgO@BPBC and f) MgO@CBC

Through EDX analysis, RHBC was found to have significant peaks corresponding to carbon (C), oxygen (O), and silicon (Si). These elements displayed respective percentage distributions of 40%, 38.7%, and 20.2%. Additionally, minor peaks were observed for potassium, calcium, magnesium, chlorine, and iron, with percentages of 0.2%, 0.2%, 0.3%, 0.1%, and 0.1%, respectively. BPBC showed peaks for carbon (C), oxygen (O), chlorine (Cl), and potassium

(K) with percentages of 49.4%, 22.9%, 7.5%, and 16.3%, respectively. In addition, minor peak values were found for calcium, magnesium, iron, and silicon at percentages of 0.7%, 1.4%, 0.9%, and 0.9%. CBC also indicated peaks for carbon (C), oxygen (O), and silicon (Si), with percentage distributions of 17.1%, 44.8%, and 31.9%, respectively. In addition, insignificant peaks were identified for chlorine, potassium, calcium, magnesium, and iron, with percentages of 0.2%, 2.8%, 0.3%, 0.7%, and 2.1%. Magnesium (Mg), oxygen (O), carbon (C), chlorine (Cl), and silicon (Si) peaks were revealed by MgO@RHBC. Their percentage distributions were 8.1%, 32.4%, 36.9%, 17.6%, and 1.3%, respectively. Iron, calcium, and potassium all showed slight peaks, with percentages of 1.1%, 0.7%, and 2%, respectively. Carbon (C), oxygen (O), magnesium (Mg), and chlorine (Cl) all showed substantial peaks in MgO@BPBC, with percentage distributions of 45%, 20.7%, 8.6%, and 20.8%, respectively. Likewise, there were negligible calcium and potassium peaks, which made up about 1.3% and 3.6% of the total. MgO@CBC uncovered prominent peaks corresponding to magnesium (Mg), oxygen (O), carbon (C), chlorine (Cl), and silicon (Si). Their respective percentage distributions were 8.8%, 33%, 40%, 12.9%, and 4.2%. Beyond that, lower peaks were identified for potassium, calcium, and iron, with percentage values of 0.1%, 0.7%, and 0.3%, respectively. The notable increase in MgO content within the MgO-modified biochar indicates that the activation process succeeded in boosting MgO levels in three modified materials, which is crucial for their intended use.

Table 4.1: EDX analysis of RBC and MgO@BC

		Weight %					
Sr. No.	Elements	RHBC	BPBC	CBC	MgO@RHBC	MgO@BPBC	MgO@CBC
1	C	40.2	49.4	17.1	36.9	45.0	40.0
2	O	38.7	22.9	44.8	32.4	20.7	33.0
3	Mg	0.3	1.4	0.7	8.1	8.6	8.8
4	Si	20.2	0.9	31.9	1.3	0.0	4.2
5	Cl	0.1	7.5	0.2	17.6	20.8	12.9
6	K	0.2	16.3	2.8	2.0	3.6	0.1
7	Ca	0.2	0.7	0.3	0.7	1.3	0.7
8	Fe	0.1	0.9	2.1	1.1	0.0	0.3

4.1.2. FT-IR analysis

The FT-IR spectra of both RBCs and MgO@BCs were recorded across the wavenumber range of 4000 to 400 cm^{-1}, as depicted in the figures. These spectra reveal distinct features for both RBCs in fig. 4.4A and MgO@BCs in fig. 4.4B. In RHBC, peaks at approximately 3419, 2920, 1613, 1095, 801 and 569 cm^{-1} shifted to around 3407, 2924, 1637, 1095, 725 and 619 cm^{-1}

respectively in MgO@RHBC. Similarly, in BPBC, peaks at 3428, 2929, 1628, 1107, and 613 cm^{-1} shifted to 3420, 2922, 1635, 1103, and 623 cm^{-1} respectively in MgO@BPBC. In CBC, peaks at 3418, 2923, 1620, 792 and 566 cm^{-1} respectively shifted to 3410, 2920, 1635, 731 and 622 cm^{-1} in MgO@CBC. In the RBC spectra, peaks at 3419 cm^{-1} for RHBC, 3428 cm^{-1} for BPBC, and 3418 cm^{-1} for CBC are indicative of the vibration stretching observed in water and alcoholic groups, confirming their presence (Priya et al. 2022b).
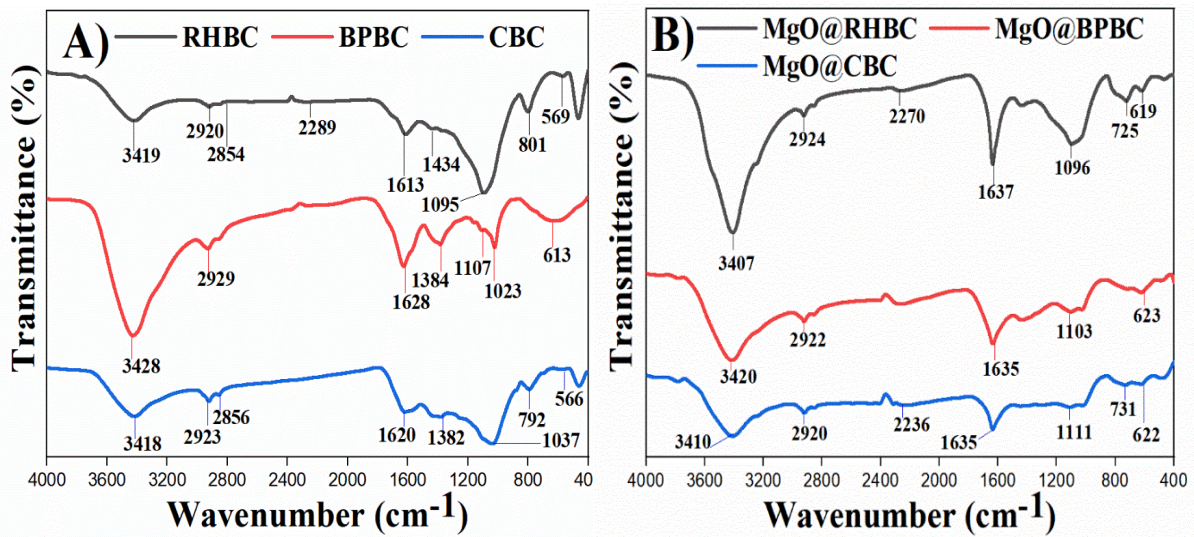

Figure 4.2: FT-IR Analysis A) RBCs and B) MgO@BCs

Particularly, the RHBC showed hydroxyl (O-H) group stretching at around 3419.48 cm^{-1}, indicating a presence that is probably related to the moisture content of the studied adsorbents (Sanka, Rwiza, and Mtei 2020b). The bands at 2920, 2929, and 2922 cm^{-1} correspond to the -CH stretching vibration of alkane groups for RHBC, BPBC, and CBC (Oladipo, Ahaka, and Gazi 2019b). Moreover, the C=C stretching of alkenes is shown by peaks for RHBC, BPBC, and CBC at 1613, 1628, and 1619 cm^{-1}. Distinct bands are visible in BPBC and CBC: the nitro compounds' -NO$_2$ bands are present at 1384 and 1382 cm^{-1}, whereas BPBC's nitrile group's C≡N stretching is seen at 2272 cm^{-1}. In the RBCs spectra, peaks ranging from 1107 to 613 cm^{-1} are observed, attributed to the formation of free alkyl and aryl groups. After modifying RHBC, BPBC, and CBC with MgO, the intensity of peaks corresponding to the amide C=O bond and the alkene C=C group at 1637, 1635.44, and 1635.15 cm^{-1} notably increased with higher Mg content in the biochar, reaching 8.1%, 8.6%, and 8.8%, respectively (J. Zhang et al. 2020a). Interestingly, the peaks at 725 cm^{-1}, 1103 cm^{-1}, and 731 cm^{-1} for MgO@RHBC, MgO@BPBC, and MgO@CBC, respectively, were lower compared to RBCs, suggesting successful coating of MgO onto the biochar surface (A. Li, Ge, et al. 2022b). The peak intensity at 3407 cm^{-1}, 3420 cm^{-1}, and 3410 cm^{-1} for MgO@RHBC, MgO@BPBC, and MgO@CBC, respectively,

decreased compared to RBC, suggesting that the presence of MgO may have led to a reduction in O-H functional groups (Qin et al. 2020).

4.1.3. XRD analysis

The XRD analysis of RBCs (fig. 4.3A) and MgO@BCs (fig. 4.3B) aimed to provide information on the crystal structure, phase composition, crystal symmetry, lattice parameters, crystal size, and orientation of the crystalline materials of the adsorbents. Diffraction peaks were detected at 2θ angles of $26.15°$, $26.6°$, and $26.4°$ for RHBC. These observations suggest crystalline structures in line with hexagonal SiO_2, SiC, and C, which correspond to planes (101), (005), and (002) and correspond with the JCPDS numbers 11-0252, 42-1360, and 41-1487. The presence of a wide and weak band around $26.4°$ at an approximate 2θ angle indicates that RHBC contains graphitic platelets. Therefore, as demonstrated by the absence of strong and identifiable peaks in the XRD investigation, the primary composition of RHBC is amorphous carbon (Amen et al. 2020). Further, in RHBC the existence of SiO_2 is shown, and its amorphous carbon nature is proven by the absence of any other prominent peaks (J. Shi et al. 2019; Scapin et al. 2021). Due to the presence of substantial amounts of quartz (SiO_2), the strong peak at $2\theta = 26.15°$ shows the importance of silica in RHBC composition (Khoshnood Motlagh, Sharifian, and Asasian-Kolur 2021; Muthukrishnan, Gupta, and Kua 2019). Peaks at 2θ angles of $66.62°$, $40.38°$, and $28.11°$ for BPBC suggest a crystalline structure of cubic Fe_2Si and C_{60}, and hexagonal FeC_8 at planes (110), (520), and (006), matching to file number 26-1141, 49-1720, and 51-0624 (Ying tao Sun et al. 2023). Further, two peaks were observed in BPBC structure suggesting the involvement of iron carbide and fullerite (Ngankam et al. 2020; Foroutan et al. 2022). CBC showed diffraction peaks at $66.42°$ and $40.41°$, confirming a cubic crystalline structure with Fe_2Si and C60 at planes (110) and (520). These results are consistent with JCPDS files 26-1141 and 49-1720. Diffraction peaks in MgO@RHBC were detected at 2θ angles of $39.39°$ and $39.22°$, $33.96°$ and $33.71°$ for C, K_6MgO_4, $MgCN_2$ and Si_3N_4, supporting a hexagonal crystalline structure at planes (111), (300), (012) and (200). It is evident that MgO is the main crystal phase in the MgO@RHBC composite, as the Mg_2Si peak at plane (220) shows a cubic crystalline structure at an angle of $39.95°$ (Xiang et al. 2018a). The MgO@BPBC composite showed peaks at 2θ angles of $27.57°$, $27.18°$ and $26.64°$, corresponding to Mg_2C_3, Si_3N_4, and C, suggesting a hexagonal crystalline structure on planes (104), (200), and (005). Diffraction peaks at 2θ angles of $39.98°$ and $37.74°$ confirm the cubic structure of Mg_2Si and Mg_3P_2 compounds in MgO@CBC at planes (220) and (222). The peak

found at 32.49° for MgP$_4$ implies a monoclinic crystalline structure at plane (111), according to JCPDS card numbers 30-0795 (Tran et al. 2022a). Following RBC modification, distinct
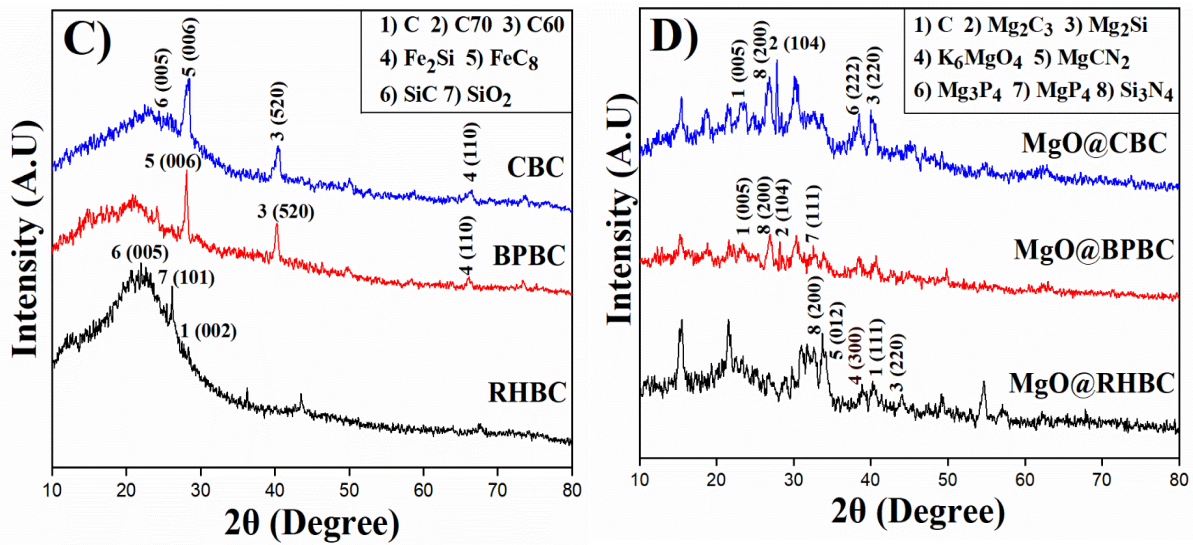

Figure 4.3: XRD analysis C) RBCs and D) MgO@BCs

MgO-related peaks appeared on the XRD patterns, suggesting an effective coating (Xu et al. 2022a). It came to light that there is an obvious link between the MgO and Mg content (J. Zhang et al. 2020b) also consistent with the EDX and SEM results (Q. Shi et al. 2021a). Comparison of the crystal structures of RBC and MgO@BC revealed changes, especially in novel peaks linked to magnesium oxide (MgO) at planes (200), (220), and (222), indicating successful MgO incorporation (Xu et al. 2022a). Ultimately, the XRD data discloses that the materials contain abundant surface functional groups that are helpful with heavy metal removal (Cheng et al. 2023). The raw biochar (RBCs) i.e. RHBC, BPBC and CBC, disclosed crystallite sizes of 0.37, 0.3 and 0.24 nm. After the modification, the crystallite sizes of MgO@RHBC, MgO@BPBC and MgO@CBC are 0.85, 3.52 and 0.99 nm, respectively (fig. 4.3D) (Zhu et al. 2020b; Tran et al. 2022b; Chaubey et al. 2023; Luna-Lama, Morales, and Caballero et al. 2021). Degrees of crystallinity were 3.05, 4.81 and 6.85% for the raw sorbents, including RHBC, BPBC and CBC. All the sorbents crystallinity improved after modifying it. The respective values for MgO@RHBC, MgO@BPBC, and MgO@CBC are 9.44, 16.72 and 15.51%.

4.1.4. Proximate analysis

Proximate analysis of RBCs and MgO@BCs was conducted to assess moisture content, volatile matter, ash, and fixed carbon content (table 4.2). The moisture content for RHBC, BPBC, and CBC was 1.4%, 11.9%, and 0.4%, respectively, while for MgO@RHBC, MgO@BPBC, and MgO@CBC, it was 9.9%, 2.73%, and 1%, respectively. The volatile matter and ash content for RHBC, BPBC, and CBC were 39.95%, 75.48%, and 47.48%, and 21.29%, 0.1%, and 18.97%,

respectively. The high ash observed in RHBC may be attributed to the presence of silica, as confirmed by EDX. This could hinder its use as an activated carbon precursor, as ash obstructs pore formation, resulting in activated carbon with low adsorption capacity (Menya et al. 2020). After modification, the volatile matter and ash content for MgO@RHBC, MgO@BPBC, and MgO@CBC were 59.48%, 60.97% and 48.98%, and 2.66%, 1.081% and 9.69%, respectively. The analysis shows that both BPBC and MgO@BPBC are dominated by volatile matter, comprising 75.48% and 60.97%, respectively. This volatile matter primarily consists of lignocellulosic components such as cellulose, hemicellulose, and lignin (Bong et al. 2022). BPBC and MgO@BPBC biochar have low ash content because banana peels naturally contain fewer inorganic minerals compared to other biomass sources. During pyrolysis, the organic matter converts to carbon, and the low mineral content results in minimal ash formation. Additionally, the high volatile organic compounds and lignocellulosic materials in banana peels decompose and volatilize during carbonization, leaving behind little ash. The fixed carbon content for RHBC, BPBC, and CBC was 38.76, 24.42 and 33.55%, and for MgO@RHBC, MgO@BPBC, and MgO@CBC, it was 37.86, 37.94 and 41.33%, respectively. This high carbon content indicates the production of desirable carbon-rich biochar.

4.1.5. BET analysis

This analysis is carried out to determine the pore radius, volume and surface area of both raw and activated biochar samples. The determined BET surface areas for RHBC, BPBC, and CBC were found to be 12.0732 m^2/g, 0.7296 m^2/g, and 7.0285 m^2/g, respectively. Specifically, the BET surface areas for MgO@RHBC, MgO@BPBC and MgO@CBC were measured as 11.1163 m^2/g, 10.1938 m^2/g and 8.9306 m^2/g, respectively. It was found that the surface area of MgO@BPBC (10.1938 m^2/g) was notably greater than BPBC (0.7296 m^2/g). Similarly, the surface area of MgO@CBC (8.9306 m^2/g) was slightly greater than CBC (7.0285 m^2/g). Previously, surface area enhancement was noted upon the modification of the adsorbent. Specifically, the surface area increased 29.12 m^2/g to 830.125 m^2/g (Xu et al. 2022a) and 5.759 m^2/g to 8.147 m^2/g (Xiao et al. 2024). The presence of MgO on the surface of the adsorbent may contribute to the observed improvement in surface characteristics, potentially enhancing its adsorption capacity over time. Physico-chemical properties of RBCs and MgO@BCs are shown in table 4.2.

Table 4.2: Physicochemical Properties of RBC and MgO@BC

Sr. No.	Material	Proximate analysis (%)				BET surface area (m²/g)	Pore volume (cm³/g)	Pore Radius (nm)
		Moisture Content	Volatile Matter	Ash	Fixed Carbon			
1	RHBC	1.4	39.95	21.29	38.76	12.0732	0.002294	2.0313
2	BPBC	11.9	75.48	0.1	24.42	0.7296	0.000174	2.0569
3	CBC	0.4	47.48	18.97	33.55	7.0285	0.002021	2.031
4	MgO@RHBC	9.9	59.48	2.66	37.86	11.1163	0.003257	2.0607
5	MgO@BPBC	2.73	60.97	1.081	37.949	10.1938	0.002052	2.0474
6	MgO@CBC	1	48.98	9.69	41.33	8.9306	0.002726	2.0553

4.2. Batch adsorption study

4.2.1. Influence of pH and dosage

The adsorbent's surface functional groups and active sites are sensitive to pH variations due to the pH-dependent nature of oxygen-containing functional groups on its surface thereby impacting adsorption performance (Hock et al. 2024; Ambaye et al. 2021). The pHpzc values of the six biochar materials were determined to be: RHBC (5.83), MgO@RHBC (9.67), BPBC (7.69), MgO@BPBC (9.55), CBC (9.04), and MgO@CBC (9.65) (Menya et al. 2022). Notably, the determined pHpzc values exceed the pH levels (2, 4) used in this study. At pH values below the pHpzc, protonation of biochar functional groups occurs ($^-OH + H^+ \rightarrow {^-OH_2}^+$), resulting in a net positive surface charge under acidic conditions. This phenomenon enhances the sorption capacity of biochar towards anionic metals (Ambaye et al. 2021). Fig. 4.4(a, b) shows the influence of dosages on chromium (VI) removal in a single solute system across six materials: RHBC, MgO@RHBC, BPBC, MgO@BPBC, CBC, and MgO@CBC. Comparison of the removal efficiency conducted with pH 2 fig. 4.4a and pH 4 fig. 4.4b. The percentage removal of Cr (VI) increased at pH 2 compared to pH 4. This is because at highly acidic pH i.e. 2, anionic Cr (VI) species ($HCrO_4^-$ and $Cr_2O_7^{2-}$) predominate, allowing strong electrostatic interaction between chromate ions and positively charged adsorbent. On the other side, pH 4 presents a distinct scenario, where reduced H^+ and increased OH^- ions facilitate competition among anionic species (Cr^{6+}) for surface binding sites, ultimately decreasing removal efficiency as shown in fig. 4.4b (Ambaye et al. 2021; Usmani et al. 2023). Fig. 4.4a, BPBC exhibited a removal efficiency of 96%, while MgO@BPBC showed a slightly higher efficiency at 97%. In contrast, CBC achieved 80.5% and MgO@CBC reached 94.3% removal at dosage of 2 g/L. Notably, increasing the dosage to 4 g/L led to decreased removal efficiencies for

BPBC, MgO@BPBC, CBC, and MgO@CBC. This behavior can be attributed to the effects of higher dosages on the material's zeta potential and destabilization potential. As the dosage increases, the overall zeta potential of the materials moves away from the isoelectric point, leading to particle destabilization and degraded adsorption properties. In contrast, the removal of Pb (II) in the single solute system under the same initial conditions exhibits an opposite trend, showing greater removal at pH 4 fig. 4.4d compared to pH 2 fig. 4.4c. At pH 2, the abundance of H^+ ions enhance the cationic properties of biochar, leading to weak complex formation and increased cationic repulsion, which reduces the removal affinity for Pb (II). Conversely, at pH 4, the decreased H^+ ions, slightly increased OH^- ions and cationic species of Pb^{2+} facilitate better charge neutralization, resulting in enhanced removal efficiency. Additionally, at pH 4, the removal of Pb (II) by BPBC decreased from 50% at 2 g/L to 0% at 4 g/L due to increased electrostatic repulsion between the positively charged biochar surface and Pb^{+2} ions at higher dosages.
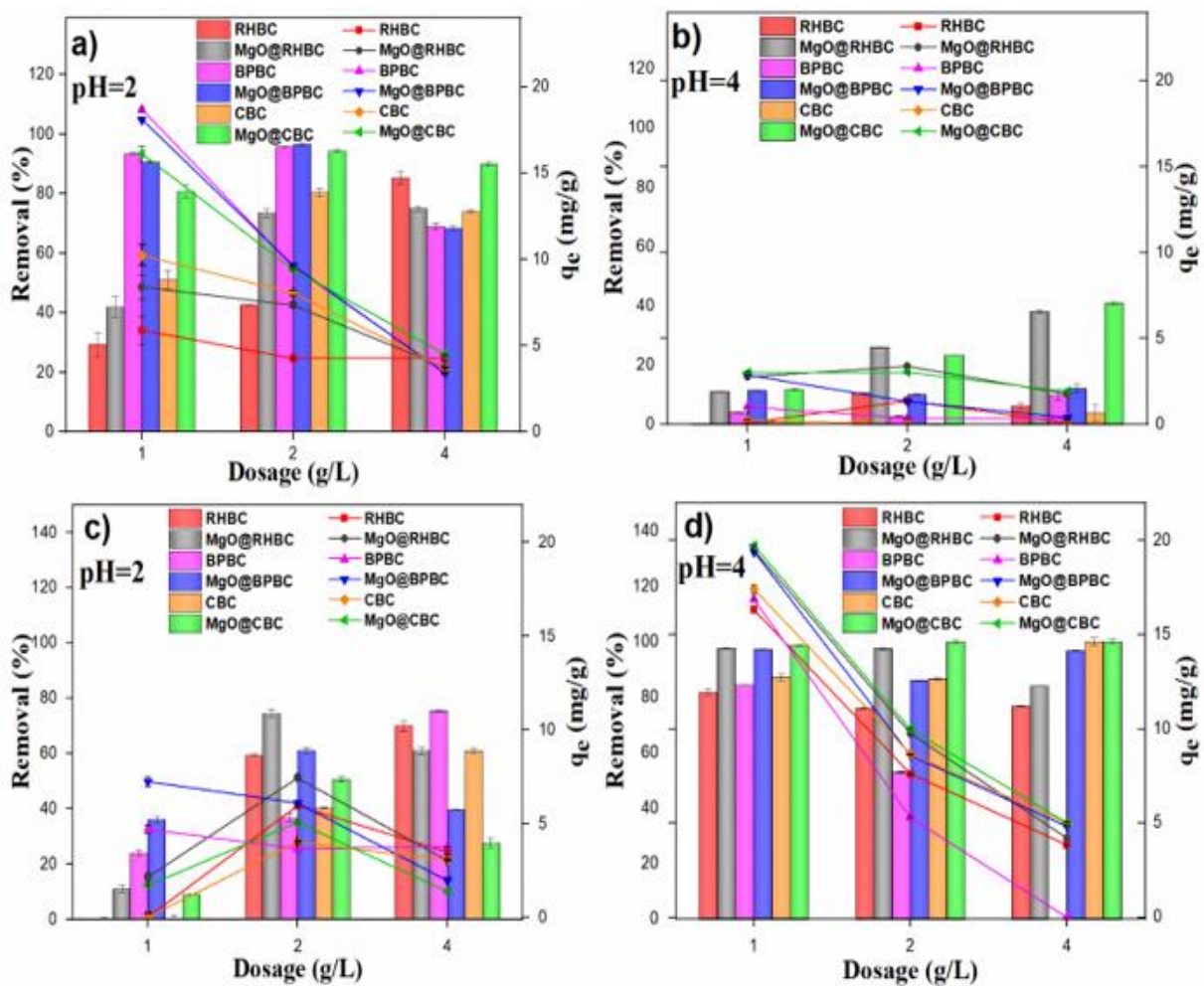

Figure 4.4: Effect of dosage on Cr (VI) removal (a, b) and Pb (II) removal (c, d)

(Single solute system)

4.2.2. Influence of initial metal concentration
4.2.2.1. Single solute system

Fig. 4.5(A, B) presents the effect of initial chromium concentration on removal percentage in a single system at pH 2 and 4, utilizing MgO@CBC dosages of 2 g/L and 4 g/L. With rising initial chromium concentrations ranging from 10 to 100 mg/L, removal efficiency declines significantly. At pH 2, removal efficiency decreases from 96 to 48% for the 2 g/L and from 95 to 60% for the 4 g/L dosage. In contrast, at pH 4, removal efficiency decreases from 30 to 0% for the 2 g/L and from 80% to 5% for the 4 g/L dosage. These findings indicate that increased dosages can offer more accessible active sites for Cr (VI) adsorption on the surface of biochar, thereby enhancing removal. Fig. 4.5(C, D) reveals a distinct trend in Pb (II) removal in a single system. At 2 g/L dosage, Pb (II) removal decreases from 55 to 12% at pH 2 and from 100 to 75% at pH 4. Conversely, at 4 g/L dosage, removal decreases from 32 to 0% at pH 2 and from 100 to 23% at pH 4. Notably, the reduced removal efficiency at pH 2 with 4 g/L dosage, compared to 2 g/L dosage, could be due to the higher dosage affecting the zeta potential of the material, thereby hindering Pb (II) adsorption.
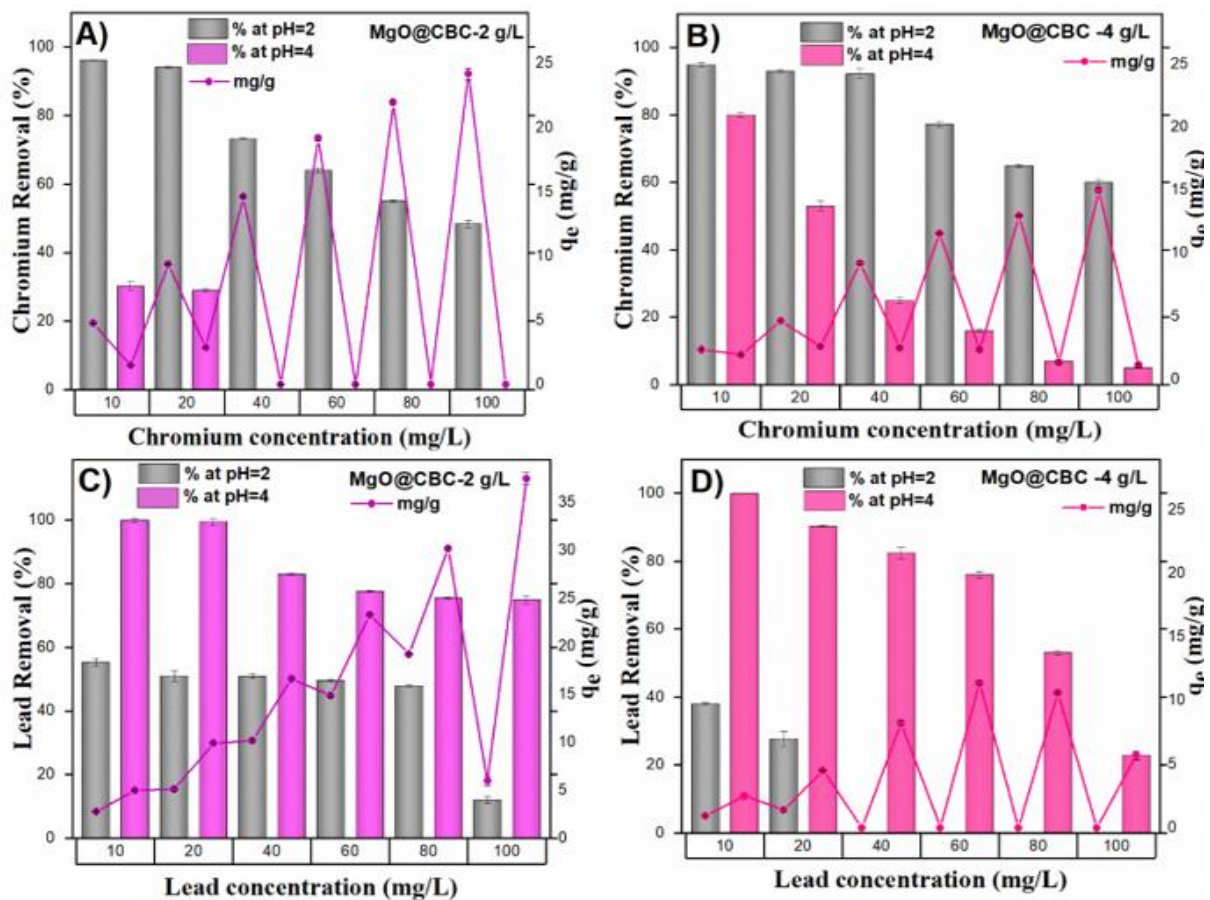

Figure 4.5: Effect of concentration on the removal of Cr (VI) (A, B) and Pb (II) (C, D)

(Single solute system)

35

4.2.2.2. Binary solute system

Fig. 4.6(A, B) illustrates the impact of a binary system on Cr (VI) removal, at 2 g/L dosage, removal decreases from 95 to 61% at pH 2 and from 32 to 11% at pH 4. Similarly, at 4 g/L dosage, removal decreases from 95 to 78% at pH 2 and from 73 to 28% at pH 4. Notably, the binary system shows greater Cr (VI) removal at pH 2, likely due to competitive adsorption and the formation of stronger complexes with enhanced charge neutralization. Fig. 4.6(C, D) presents the Pb (II) removal in the same binary solute, at 2 g/L dosage, removal decreases from 99 to 69% at pH 2 and from 87 to 48% at pH 4. At 4 g/L removal decreases from 100 to 76% at pH 2. As with Cr (VI) at pH 2, the binary system outperforms the single system in Pb (II) removal at both pH 2 and 4, due to the synergistic removal effect and competitive adsorption influenced by Cr (VI) species. Moreover, consistent with previous research (Amin, Alazba, and Shafiq 2018a), high initial concentrations compromise removal efficiency by causing rapid binding site saturation and adsorbent surface overload, limiting adsorption capacity.
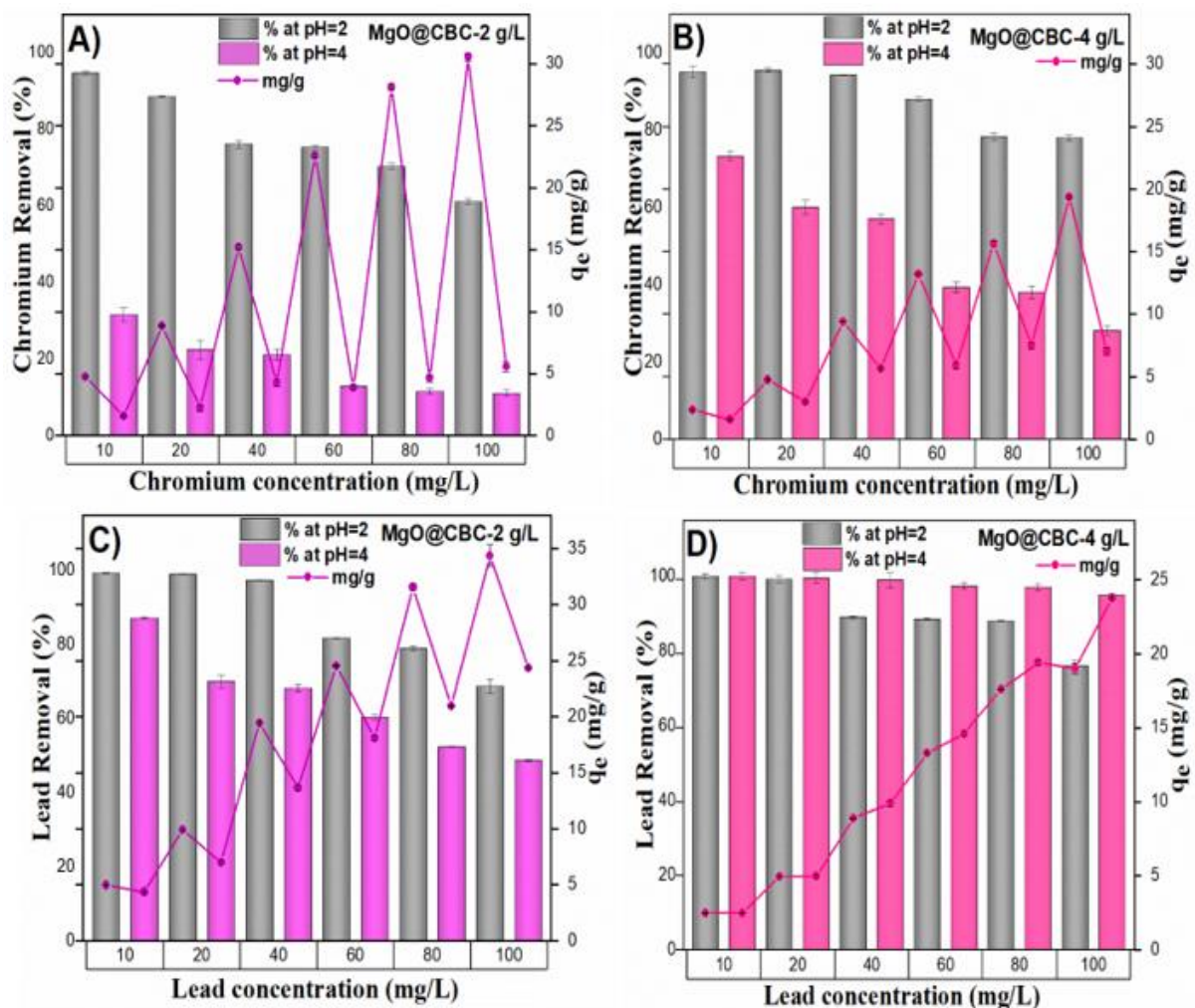

Figure 4.6: Effect of concentration on the removal of Cr (VI) (A, B) and Pb (II) (C, D)

(Binary solute system)

4.3. Adsorption isotherm study

The adsorption behavior was investigated using langmuir and freundlich non-linearized isotherm models. In single solute freundlich model ($R^2 = 0.984$) provides a better fit than the langmuir ($R^2 = 0.722$) for describing Cr (VI) adsorption at pH 2 and 2 g/L dosage (fig. 4.7a). In contrast, fig. 4.7b shows that neither model accurately fits at pH 4. This observation aligns with previous studies that reported challenges in obtaining reliable adsorption isotherm parameters for similar anionic species, such as arsenic (V) (Inam et al. 2018). For Pb (II) at pH 2 fig. 4.7c, experimental data significantly deviates from both models, showing scattered points. At pH 4 fig. 4.7d, the freundlich ($R^2 = 0.837$) and langmuir ($R^2 = 0.712$) models at 2 g/L provide moderate fits, capturing some but not all adsorption mechanisms.

Whereas in a binary solute system, the adsorption behavior of Cr (VI) shows a good fit to both the langmuir and freundlich model. The langmuir yields R^2 values of 0.937 at pH 2 (fig. 4.7e) and 0.901 at pH 4 (fig. 4.7f) at a dosage of 2 g/L, while freundlich provides R^2 values of 0.966 at pH 2 and 0.985 at pH 4. This indicates that multiple contaminants enhance adsorption, with both monolayer and multilayer sorption being effectively captured (Liang et al. 2023). A similar trend is observed for Pb (II) in the same system, where the langmuir gives R^2 values of 0.862 at pH 2 (fig. 4.7g) and 0.908 at pH 4 (fig. 4.7h), while the freundlich achieves R^2 values of 0.936 at pH 2 and 0.965 at pH 4. The freundlich model surpasses langmuir in simulating lead sorption, indicating multilayer adsorption and providing a better fit and more accurate interpretation (Ashfaq et al. 2021). All variables and their values are listed in table 4.3.
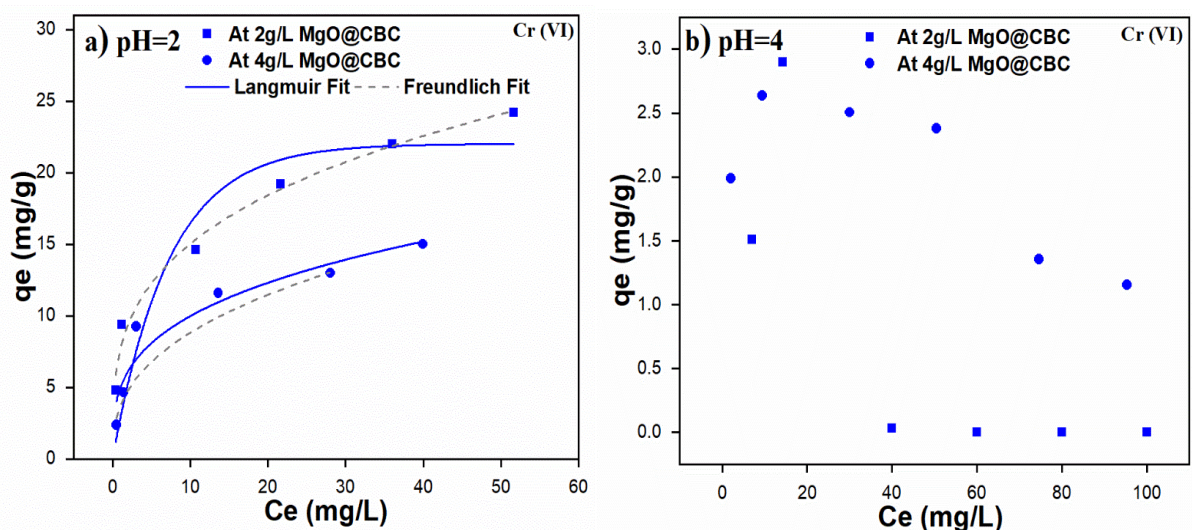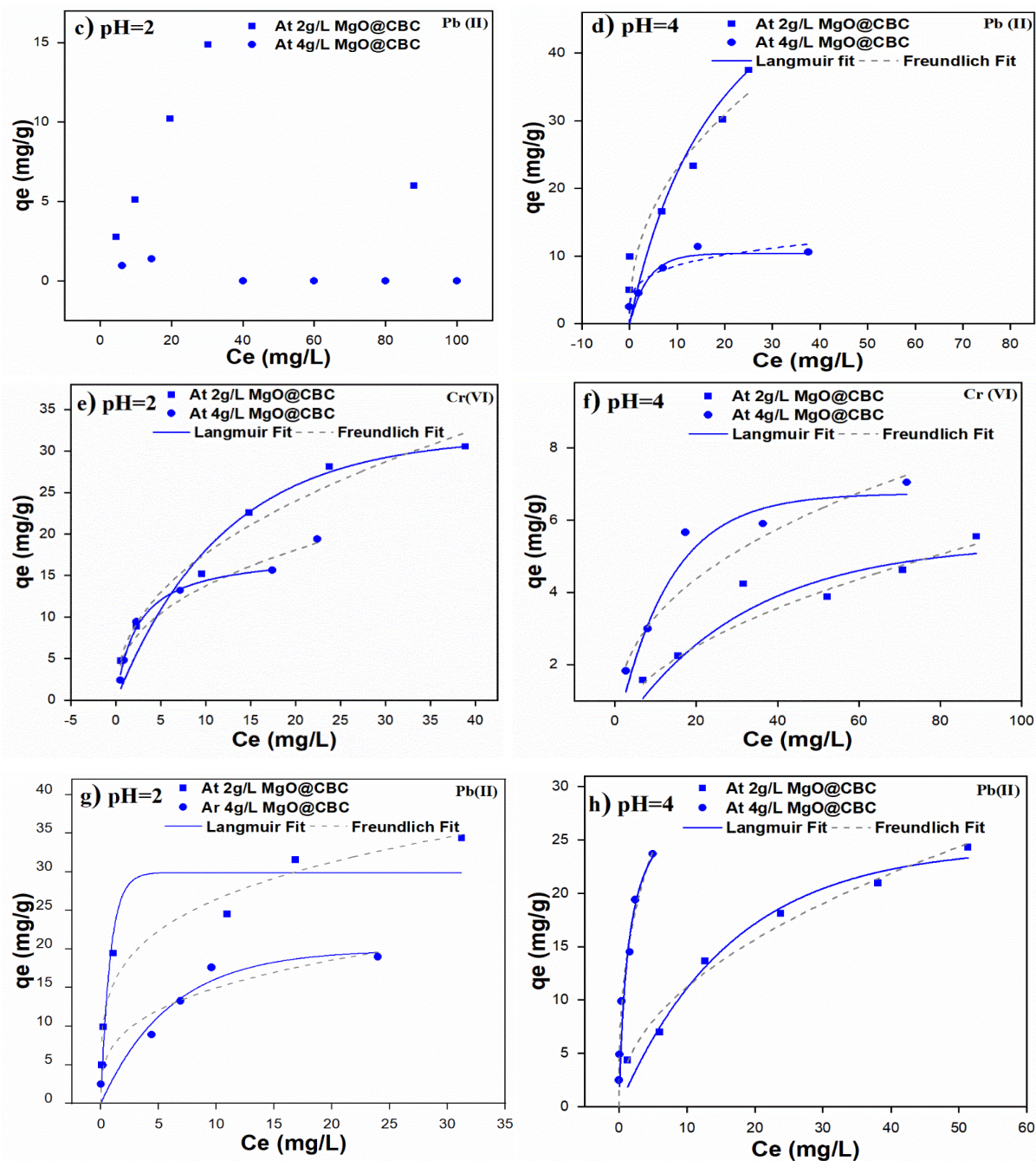
Figure 4.7: Isotherm studies of MgO@CBC

Single solute (a, b, c, d) and binary solute (e, f, g, h)

Table 4.3: Isotherm parameters

Chromium(VI) pH=2 SS		Graph (a)
Model	**Langmuir Fitting**	
Equation	$q_e=(q_mKC_e)/(1+(KC_e))$	
Plot	At 2g/L MgO@CBC$_{Cr-Pb}$	At 4g/L MgO@CBC$_{Cr-Pb}$
q_m (g/mol)	22.02	13.30
k_L (L/mg)	0.137	0.34
R^2	0.722	0.935
Model	**Freundlich Fitting**	

Equation	$q_e = K(C_e^{(1/n)})$	
Plot	At 2g/L MgO@CBC$_{Cr-Pb}$	At 4g/L MgO@CBC$_{Cr-Pb}$
Kf (L/mg)	7.65	3.67
N	3.41	2.63
R^2	0.984	0.987

Lead(II) pH=4 SS **Graph (d)**

Model	Langmuir Fitting	
Equation	$q_e = (qmKC_e)/(1+(KC_e))$	
Plot	At 2g/L MgO@CBC$_{Pb}$	At 4g/L MgO@CBC$_{Pb}$
q_m (g/mol)	68.12	10.41
k_L (L/mg)	0.048	0.257
R^2	0.712	0.748
Model	Freundlich Fitting	
Equation	$q_e = K(C_e^{(1/n)})$	
Plot	At 2g/L MgO@CBC$_{Pb}$	At 4g/L MgO@CBC$_{Pb}$
Kf (L/mg)	8.48	4.98
N	2.31	4.20
R^2	0.837	0.695

Chromium(VI) pH=2 BS **Graph (e)**

Model	Langmuir Fitting	
Equation	$q_e = (qmKC_e)/(1+(KC_e))$	
Plot	At 2g/L MgO@CBC$_{Cr-Pb}$	At 4g/L MgO@CBC$_{Cr-Pb}$
q_m (g/mol)	31.745	17.84
k_L (L/mg)	0.084	0.41
R^2	0.937	0.989
Model	Freundlich Fitting	
Equation	$q_e = K(C_e^{(1/n)})$	
Plot	At 2g/L MgO@CBC$_{Cr-Pb}$	At 4g/L MgO@CBC$_{Cr-Pb}$
Kf (L/mg)	6.36	5.54
N	2.25	2.51
R^2	0.966	0.939

Chromium(VI) pH=4 BS **Graph (f)**

Model	Langmuir Fitting	
Equation	$q_e = (qmKC_e)/(1+(KC_e))$	
Plot	At 2g/L MgO@CBC$_{Cr-Pb}$	At 4g/L MgO@CBC$_{Cr-Pb}$
q_m (g/mol)	5.38	6.73
k_L (L/mg)	0.032	0.076
R^2	0.901	0.946
Model	Freundlich Fitting	
Equation	$q_e = K(C_e^{(1/n)})$	
Plot	At 2g/L MgO@CBC$_{Cr-Pb}$	At 4g/L MgO@CBC$_{Cr-Pb}$
Kf (L/mg)	0.553	1.33
N	1.98	2.53
R^2	0.985	0.983

Lead(II) pH=2 BS **Graph (g)**

Model	Langmuir Fitting	
Equation	$q_e = (qmKC_e)/(1+(KC_e))$	
Plot	At 2g/L MgO@CBC$_{Cr-Pb}$	At 4g/L MgO@CBC$_{Cr-Pb}$

q_m (g/mol)	29.88	19.88
k_L (L/mg)	1.22	0.167
R^2	0.862	0.825
Model	**Freundlich Fitting**	
Equation	$q_e = K(C_e^{(1/n)})$	
Plot	At 2g/L MgO@CBC$_{Cr-Pb}$	At 4g/L MgO@CBC$_{Cr-Pb}$
Kf (L/mg)	15.16	7.36
N	4.14	3.24
R^2	0.936	0.874
Lead(II) pH=4 BS		**Graph (h)**
Model	**Langmuir Fitting**	
Equation	$q_e = (qmKC_e)/(1+(KC_e))$	
Plot	At 2g/L MgO@CBC$_{Cr-Pb}$	At 4g/L MgO@CBC$_{Cr-Pb}$
q_m (g/mol)	30.04	24.41
k_L (L/mg)	0.708	0.06
R^2	0.908	0.962
Model	**Freundlich Fitting**	
Equation	$q_e = K(C_e^{(1/n)})$	
Plot	At 2g/L MgO@CBC$_{Cr-Pb}$	At 4g/L MgO@CBC$_{Cr-Pb}$
Kf (L/mg)	13.14	3.69
N	2.66	2.07
R^2	0.965	0.976

4.4. Removal mechanism

The mechanism for detecting phase transitions in MgO@CBC samples after contaminant adsorption at pH (2, 4) illustrated in fig. 4.8 FTIR (a, b); XRD (c, d). After adsorption, the MgO diffraction peak significantly weakened as an indication of its participation (Q. Shi et al. 2021b), indicating replacement by strongly bonded HM-O groups via ligand exchange, ion exchange, and complexation (Xiang et al. 2018b; Kuang et al. 2019). At pH 2 (fig. 4.8a) detected HM-O groups at specific wavenumbers: (799, 499) cm^{-1} in AR: MgO@CBC$_{Cr}$, 803 cm^{-1} in AR: MgO@CBC$_{Pb}$, and (799, 473) cm^{-1} in AR: MgO@CBC$_{Cr-Pb}$. At pH 4 (fig, 4.8b), HM-O stretching was observed at 475 cm^{-1} (AR: MgO@CBC$_{Cr}$), 801 cm^{-1} (AR: MgO@CBC$_{Pb}$), and 798 cm^{-1} (AR: MgO@CBC$_{Cr-Pb}$) (Anandhan et al. 2019). Moreover, at pH 4, the FTIR spectrum of AR: MgO@CBC$_{Cr}$ also showed a peak of Mg (OH) stretching at 475 cm^{-1}, indicating MgO protonation to form Mg(OH)$^+$ (MgO + H$_2$O → Mg(OH)$^+$ + H$^+$) (Liang et al. 2023; A. Li, Ge, et al. 2022c) suggesting hydroxyl groups are involved in adsorption (Kuang et al. 2019). The bands at 1430 and 1431 cm^{-1} in AR: MgO@CBC$_{Pb}$ and AR: MgO@CBC$_{Cr}$ (fig. 4.8b) represented the vibration of –COOH groups, meanwhile the peak at 1405 cm^{-1} in AR: MgO@CBC$_{Cr-Pb}$ corresponded to the carbonyl groups (O=C–O) in biochar (Liang et al. 2023). Oxygen-rich functional groups on biochar contribute a vital role in the

capture of lead (Pb^{2+}) ions (Cheng et al. 2022c). The adsorption phenomenon involved two main mechanisms: the bonding between numerous functional groups on MgO@CBC and heavy metals (Pb, Cr), and the interaction with π electrons that helped metal ions bind to biochar (Qi et al. 2022). XRD analysis of AR: MgO@CBC$_{Cr}$ at pH 2 revealed the presence of chromium silicide and magnesium chromate at planes (210) and (220) in fig.4.8c. Similarly, AR: MgO@CBC$_{Pb}$ showed the presence of lead oxide and magnesium lead at planes (212) and (111).

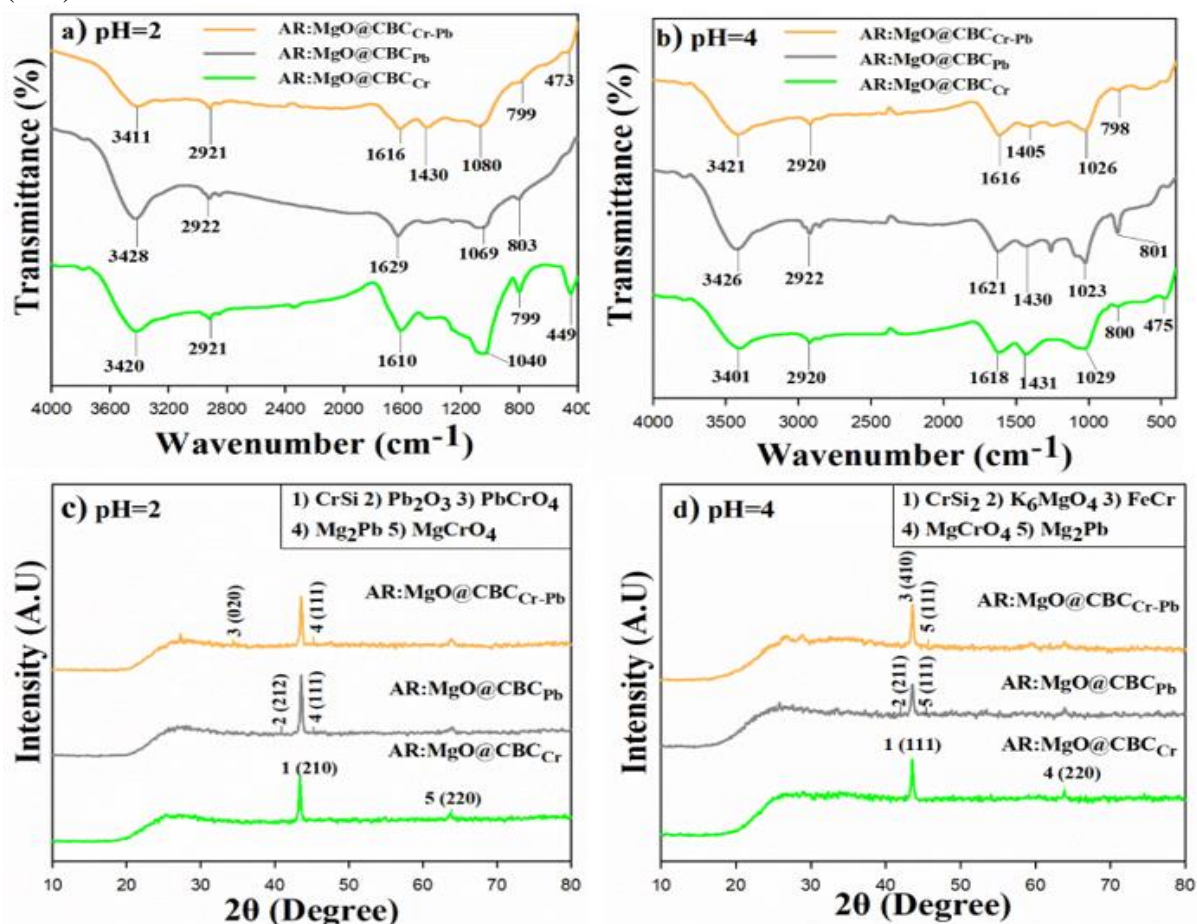Figure 4.8: After removal analysis of MgO@CBC: FTIR (a, b); XRD (c, d)

Notably, AR: MgO@CBC$_{Cr-Pb}$ depicted the presence of lead chromate and magnesium lead at planes (020) and (111) (JCPDS file #: 22-0385, 01-0465). In fig. 4.8d, at pH 4, XRD analysis of AR: MgO@CBC$_{Cr}$ revealed the presence of chromium disilicide and magnesium chromate at planes (111) and (220). AR: MgO@CBC$_{Pb}$ showed the presence of potassium magnesium oxide and magnesium lead at planes (211) and (111). Furthermore, AR: MgO@CBC$_{Cr-Pb}$ depicted the presence of ferrochromium and magnesium lead at planes (410) and (111) (L. Zhang et al. 2014). The formation of CrSi at pH 2 can be attributed to a reduction mechanism, wherein chromate is reduced to Cr^{3+} (Eq. 12), followed by its reaction with silicon from the

biochar to form chromium silicide (Eq. 13). The formation of Pb_2O_3 at pH 2 may occur via an oxidation mechanism, involving the oxidation of Pb^{2+} ions (Eq. 14). At pH 4, the formation of $CrSi_2$ could occur through a reduction mechanism, like CrSi, involving the reaction of chromate with two silicon atoms (Eq. 15). $MgCrO_4$ forms at both pH (2, 4) through surface complexation involving the interaction of magnesium oxide with chromate (Eq. 16) (H. Liu et al. 2021; Qi et al. 2022). Mg_2Pb may occur by cation exchange, which involves the chemical reaction of MgO with ions of Pb^{2+} (Eq. 17). Finally, $PbCrO_4$ forms at pH 2 resulting from electrostatic attraction, involving the reaction of Pb^{2+} ion with chromate ion (Eq. 18) (Cheng et al. 2022c). Fig. 4.9 illustrates the proposed adsorption mechanism of Pb (II) and Cr (VI) removal by MgO@CBC.
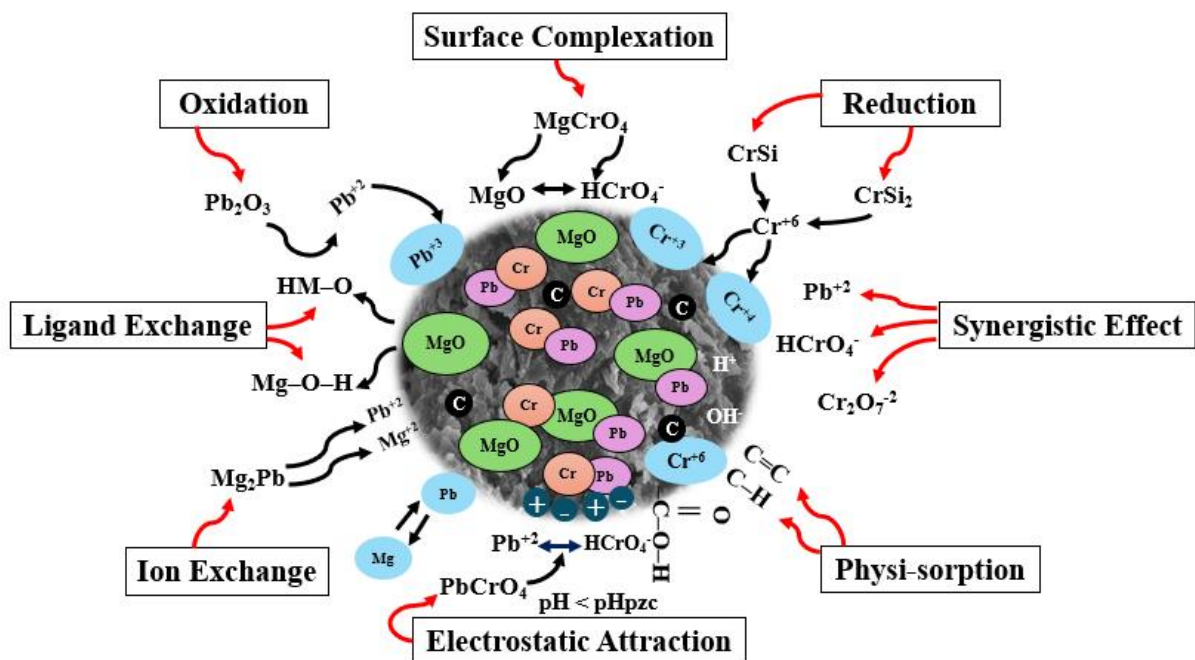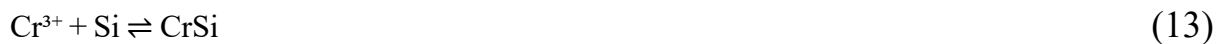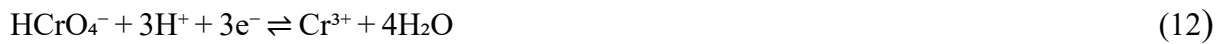
Reactions:

$$HCrO_4^- + 3H^+ + 3e^- \rightleftharpoons Cr^{3+} + 4H_2O \tag{12}$$

$$Cr^{3+} + Si \rightleftharpoons CrSi \tag{13}$$

$$2Pb^{2+} + 2OH^- \rightleftharpoons Pb_2O_3 + H_2O \tag{14}$$

$$HCrO_4^- + 4H^+ + 2Si \rightleftharpoons CrSi_2 + 4H_2O \tag{15}$$

$$MgO + HCrO_4^- \rightleftharpoons MgCrO_4 + H_2O \tag{16}$$

$$2MgO + Pb^{2+} \rightleftharpoons Mg_2Pb + O^{2-} \tag{17}$$

$$Pb^{2+} + HCrO_4^- \rightleftharpoons PbCrO_4 \tag{18}$$

Figure 4.9: Proposed adsorption mechanism of Pb (II) and Cr (VI) removal by MgO@CBC

4.5. Regeneration of MgO@CBC

The recyclability of MgO@CBC was evaluated through a series of adsorption-desorption experiments, utilizing 1.0 M NaOH as the desorbing agent for lead and chromium in both solute systems (T. Liu et al. 2022). The performance of MgO@CBC (fig. 4.10) reveals a gradual decline in removal efficiency (%) and adsorption capacity (mg/g) over five cycles. For Pb (II), efficiency decreased from 100 to 20.89% (single solute) and 99 to 0% (binary solute). Similarly, Cr (VI) removal decreased from 94 to 19.46% (single solute) and 88.5 to 6.1% (binary solute). This decrease is attributed to key factors: (1) progressive deactivation of active sites hindering Pb (II) and Cr (VI) binding upon regeneration, (2) ion exchange-mediated MgO content diminution during adsorption-desorption cycles (Cheng et al. 2022d), (3) surface property alterations caused by Pb (II) and Cr (VI) accumulation (Gkika et al. 2022), and (4) surface degradation and pore blockage due to repeated use (Xu et al. 2022b). Furthermore, a synergistic removal effect was observed during regeneration in the binary solute system. The findings indicate that MgO@CBC good reusability and metal removal capabilities make it a sustainable adsorbent for the removal of multiple metals from industrial wastewater.
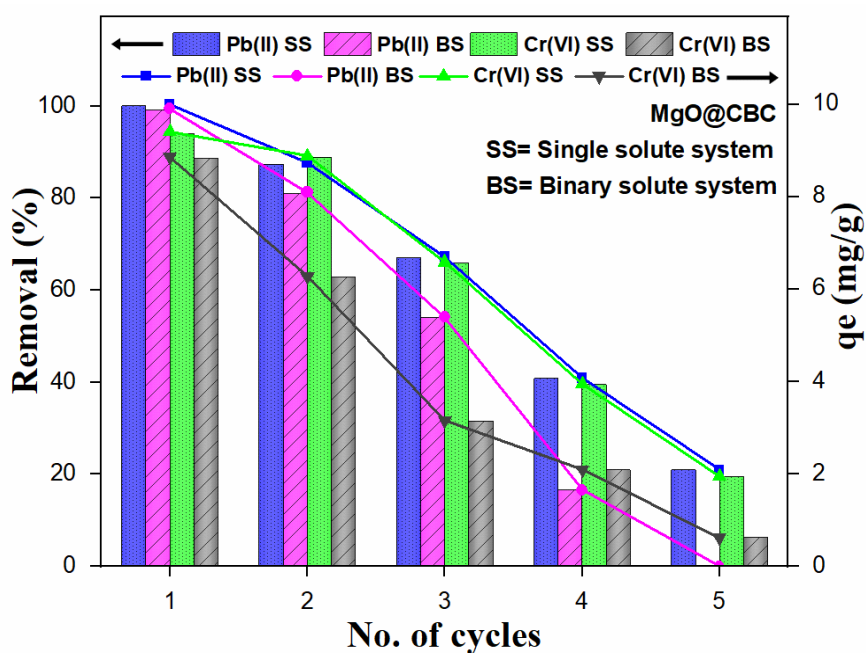

Figure. 4.10: Regeneration cycles of Cr and Pb loaded MgO@CBC in single and binary systems

<div align="right">

CHAPTER 5

</div>

CONCLUSION AND RECOMMENDATIONS

5.1. Conclusion

In this study, MgO@CBC, derived from rice husk and banana peel, features a unique combination of carbon richness and a silica-based structure, with Mg^{2+} ions playing a prominent role in the adsorption of both targeted metal ions.

Key outcomes are summarized below:

- SEM analysis revealed structural changes in MgO@CBC compared to CBC. EDX analysis showed a significant increase in Mg content with a value of 8.8% for MgO@CBC, respectively, up from 0.7 CBC.

- FTIR spectra of the MgO@CBC exhibited an absorption peak characteristic of Mg-O functional groups where XRD analysis confirms the presence of magnesium-related crystalline phases in MgO@CBC.

- MgO@CBC showed enhanced degree of crystallinity value (15.51%) exceeding CBC by 6.85% and highlighted enlarged crystallite size in MgO@CBC to 0.99 nm, surpassing CBC by 0.24 nm, indicating well-defined crystal structure formation and enhanced growth.

- The BET analysis revealed that MgO@CBC has a larger pore volume (0.002726 cm³/g) compared to CBC (0.002021 cm³/g), representing a 35% increase. Proximate analysis showed that MgO@CBC contains a higher fixed carbon content (41.33%) than CBC (33.55%) and a lower ash content (9.69% for MgO@CBC vs. 18.97% for CBC). This enhanced pore volume, increased fixed carbon, and reduced ash content due to Mg deposition contribute to the superior adsorption capacity of MgO@CBC for chromium (Cr) and lead (Pb).

- The experimental results in the single-solute system demonstrated that Cr (VI) removal reached 94% at pH 2 due to the predominant anionic Cr species, which enabled strong electrostatic interactions with the positively charged surface of MgO@CBC (greater pHpzc). In contrast, Pb (II) removal achieved 100% at pH 4, using an initial concentration of 20 mg/L and a 2 g/L MgO@CBC dosage, attributed to the reduction in H^+ ions and a slight increase in OH^- ions, cationic species of Pb^{+2} promoting better charge neutralization and enhancing removal efficiency.

- In a binary solute system, MgO@CBC achieved 88.5% Cr (VI) and 99% Pb (II) removal at 20 mg/L, pH 2, and a 2 g/L dosage. A synergistic effect for Pb (II) was observed at pH 2, where the presence of chromium species contributed to a cumulative effect, improving surface properties, enhancing charge neutralization, and boosting overall removal efficiency.

- Adsorption isotherm analysis revealed that both langmuir and freundlich models effectively describe Cr (VI) and Pb (II) adsorption in binary solute systems. Cr (VI) adsorption accurately modelled by langmuir (R^2 = 0.937, pH 2; 0.901, pH 4) and freundlich (R^2 = 0.966, pH 2; 0.985, pH 4) equations. Pb (II) adsorption also showed good fits for langmuir (R^2 = 0.862, pH 2; 0.908, pH 4) and freundlich (R^2 = 0.936, pH 2; 0.965, pH 4) models. These findings indicate that multiple contaminants promote adsorption via combined monolayer and multilayer sorption.

- The removal mechanism of Cr (VI) and Pb (II) by MgO@CBC is multifaceted, involving charge neutralization, ion exchange, ligand exchange, complexation, and oxidation-reduction reactions. The weakening of Mg-O bonds post-adsorption indicates MgO active involvement in the process. This synergistic interplay between MgO and CBC functional groups optimizes the removal of both Cr and Pb from wastewater.

- The regeneration performance of MgO@CBC showed a gradual decline in removal efficiency (%) and adsorption capacity (mg/g) over five cycles in both single and binary solute systems. This reduction is attributed to the deactivation of active sites, depletion of MgO content through ion exchange, surface degradation, and pore blockage from repeated use.

5.2. Recommendations
This research study recommends that:

- Treatment trials must be conducted in a continuous adsorption system, utilizing the current study

- Material can be used across various industries, so optimizing the removal process using statistical tools & evaluating long-term operation, accessibility & sustainability are essential

- Techno-economic analysis of the material for tannery wastewater treatment should be conducted, and its cost should be compared to current practices, such as membrane-based system.

REFERENCES

Abdelkader, S. E., A. S. El-Gendy, and S. El-Haggar. 2021. "Removal of Trivalent Chromium from Tannery Wastewater Using Solid Wastes." *Innovative Infrastructure Solutions* 6 (2). https://doi.org/10.1007/s41062-020-00414-8.

Adewuyi, Adewale. 2020. "Chemically Modified Biosorbents and Their Role in the Removal of Emerging Pharmaceuticalwaste in the Water System." *Water (Switzerland)*. MDPI AG. https://doi.org/10.3390/W12061551.

Afolabi, Felicia O., Paul Musonge, and Babatunde F. Bakare. 2021. "Evaluation of Lead (Ii) Removal from Wastewater Using Banana Peels: Optimization Study." *Polish Journal of Environmental Studies* 30 (2): 1487–96. https://doi.org/10.15244/pjoes/122449.

Agrafioti, Evita, Dimitrios Kalderis, and Evan Diamadopoulos. 2014. "Arsenic and Chromium Removal from Water Using Biochars Derived from Rice Husk, Organic Solid Wastes and Sewage Sludge." *Journal of Environmental Management* 133 (January):309–14. https://doi.org/10.1016/j.jenvman.2013.12.007.

Ahmad, Rehan, Shafaqat Ali, Muhammad Rizwan, Muhammad Dawood, Mujahid Farid, Afzal Hussain, Leonard Wijaya, Mohammed Nasser Alyemeni, and Parvaiz Ahmad. 2020. "Hydrogen Sulfide Alleviates Chromium Stress on Cauliflower by Restricting Its Uptake and Enhancing Antioxidative System." *Physiologia Plantarum* 168 (2): 289–300. https://doi.org/10.1111/ppl.13001.

Akhtar, Naseem, Muhammad Izzuddin Syakir Ishak, Showkat Ahmad Bhawani, and Khalid Umar. 2021. "Various Natural and Anthropogenic Factors Responsible for Water Quality Degradation: A Review." *Water (Switzerland)*. MDPI. https://doi.org/10.3390/w13192660.

Akter, Sonia, Md Burhan Kabir Suhan, and Md Shahinoor Islam. 2022. "Recent Advances and Perspective of Electrocoagulation in the Treatment of Wastewater: A Review." *Environmental Nanotechnology, Monitoring and Management*. Elsevier B.V. https://doi.org/10.1016/j.enmm.2022.100643.

Alalwan, Hayder A., Mohammed A. Kadhom, and Alaa H. Alminshid. 2020. "Removal of Heavy Metals from Wastewater Using Agricultural Byproducts." *Journal of Water Supply: Research and Technology - AQUA* 69 (2): 99–112. https://doi.org/10.2166/aqua.2020.133.

Alemu, Tadesse, Eshetu Lemma, Andualem Mekonnen, and Seyoum Leta. 2016. "Performance of Pilot Scale Anaerobic-SBR System Integrated with Constructed Wetlands for the Treatment of Tannery Wastewater." *Environmental Processes* 3 (4): 815–27. https://doi.org/10.1007/s40710-016-0171-1.

Alvarez, Carla Cedillo, María Elena Bravo Gómez, and Araceli Hernández Zavala. 2021. "Hexavalent Chromium: Regulation and Health Effects." *Journal of Trace Elements in Medicine and Biology*. Elsevier GmbH. https://doi.org/10.1016/j.jtemb.2021.126729.

Ambaye, T. G., M. Vaccari, E. D. van Hullebusch, A. Amrane, and S. Rtimi. 2021. "Mechanisms and Adsorption Capacities of Biochar for the Removal of Organic and Inorganic Pollutants from Industrial Wastewater." International Journal of Environmental Science and Technology. Springer Science and Business Media Deutschland GmbH. https://doi.org/10.1007/s13762-020-03060-w.

Amen, Rabia, Muhammad Yaseen, Ahmad Mukhtar, Jiří Jaromír Klemeš, Sidra Saqib, Sami Ullah, Abdullah G. Al-Sehemi, et al. 2020. "Lead and Cadmium Removal from Wastewater Using Eco-Friendly Biochar Adsorbent Derived from Rice Husk, Wheat Straw, and Corncob." Cleaner Engineering and Technology 1 (December). https://doi.org/10.1016/j.clet.2020.100006.

Amin, M. T., A. A. Alazba, and M. Shafiq. 2018. "Removal of Copper and Lead Using Banana Biochar in Batch Adsorption Systems: Isotherms and Kinetic Studies." Arabian Journal for Science and Engineering 43 (11): 5711–22. https://doi.org/10.1007/s13369-017-2934-z.

Anandhan, K., S. Harish, and R. Thilak Kumar. 2019. "Effect of Morphology on the Formation of CdO Nanostructures for Antibacterial and Hemolytic Studies." Applied Surface Science 489 (September):262–68. https://doi.org/10.1016/j.apsusc.2019.05.172.

Annadurai, G, R S Juang, and D J Lee. 2002. "Adsorption of Heavy Metals from Water Using Banana and Orange Peels." https://iwaponline.com/wst/article-pdf/47/1/185/44751/185.pdf.

Ashfaq, Aamna, Razyia Nadeem, Shamsa Bibi, Umer Rashid, Asif Hanif, Nazish Jahan, Zeeshan Ashfaq, Zubair Ahmed, Muhammad Adil, and Maleeha Naz. 2021. "Efficient Adsorption of Lead Ions from Synthetic Wastewater Using Agrowaste-Based Mixed Biomass (Potato Peels and Banana Peels)." Water (Switzerland) 13 (23). https://doi.org/10.3390/w13233344.

Asrari, *, Elham ; Tavallali, and Hossein ; Hagshenas. 2010. "Removal of Zn(II) and Pb (II) Ions Using Rice Husk in Food Industrial Wastewater." J. Appl. Sci. Environ. Manage 14 (4): 159–62. www.bioline.org.br/ja.

Ayele, Abate, and Yakob Godebo Godeto. 2021. "Bioremediation of Chromium by Microorganisms and Its Mechanisms Related to Functional Groups." Journal of Chemistry. Hindawi Limited. https://doi.org/10.1155/2021/7694157.

Ayub, Sohail, Asif Ali Siddique, Md S. Khursheed, Ahmad Zarei, Izhar Alam, Esrafil Asgari, and Fazlollah Changani. 2020. "Removal of Heavy Metals (Cr, Cu, and Zn) from Electroplating Wastewater by Electrocoagulation and Adsorption Processes." Desalination and Water Treatment 179 (March):263–71. https://doi.org/10.5004/dwt.2020.25010.

Bakatula, Elisee Nsimba, Dominique Richard, Carmen Mihaela Neculita, and Gerald J. Zagury. 2018. "Determination of Point of Zero Charge of Natural Organic Materials." Environmental Science and Pollution Research 25 (8): 7823–33. https://doi.org/10.1007/s11356-017-1115-7.

Bazrafshan, Edris, Leili Mohammadi, Alireza Ansari-Moghaddam, and Amir Hossein Mahvi. 2015. "Heavy Metals Removal from Aqueous Environments by Electrocoagulation Process - A Systematic Review." Journal of Environmental Health Science and Engineering. BioMed Central Ltd. https://doi.org/10.1186/s40201-015-0233-8.

Benalia, Mohamed Charif, Leila Youcef, Mohamed Ghrissi Bouaziz, Samia Achour, and Hayet Menasra. 2022. "Removal of Heavy Metals from Industrial Wastewater by Chemical Precipitation: Mechanisms and Sludge Characterization." Arabian Journal for Science and Engineering 47 (5): 5587–99. https://doi.org/10.1007/s13369-021-05525-7.

Bong, Hong Kai, Anurita Selvarajoo, and Senthil Kumar Arumugasamy. 2022. "Stability of Biochar Derived from Banana Peel through Pyrolysis as Alternative Source of Nutrient in Soil: Feedforward Neural Network Modelling Study." Environmental Monitoring and Assessment 194 (2). https://doi.org/10.1007/s10661-021-09691-x.

Bouida, Leila, Mohd Rafatullah, Abdelfateh Kerrouche, Mohammad Qutob, Abeer M. Alosaimi, Hajer S. Alorfi, and Mahmoud A. Hussein. 2022. "A Review on Cadmium and Lead Contamination: Sources, Fate, Mechanism, Health Effects and Remediation Methods." Water (Switzerland). MDPI. https://doi.org/10.3390/w14213432.

Burakov, Alexander E., Evgeny V. Galunin, Irina V. Burakova, Anastassia E. Kucherova, Shilpi Agarwal, Alexey G. Tkachev, and Vinod K. Gupta. 2018. "Adsorption of Heavy Metals on Conventional and Nanostructured Materials for Wastewater Treatment Purposes: A Review." Ecotoxicology and Environmental Safety. Academic Press. https://doi.org/10.1016/j.ecoenv.2017.11.034.

Chai, Wai Siong, Wee Gee Tan, Heli Siti Halimatul Munawaroh, Vijai Kumar Gupta, Shih Hsin Ho, and Pau Loke Show. 2021. "Multifaceted Roles of Microalgae in the Application of Wastewater Biotreatment: A Review." Environmental Pollution 269 (January). https://doi.org/10.1016/j.envpol.2020.116236.

Chaubey, Abhishek Kumar, Manvendra Patel, Charles U. Pittman, and Dinesh Mohan. 2023. "Acetaminophen and Trimethoprim Batch and Fixed-Bed Sorption on MgO/Al2O3-Modified Rice Husk Biochar." Colloids and Surfaces A: Physicochemical and Engineering Aspects 677 (November). https://doi.org/10.1016/j.colsurfa.2023.132263.

Cheng, Song, Weibo Meng, Baolin Xing, Changliang Shi, Qiang Wang, Daping Xia, Yanhe Nie, Gunyun Yi, Chuanxiang Zhang, and Hongying Xia. 2023. "Efficient Removal of Heavy Metals from Aqueous Solutions by Mg/Fe Bimetallic Oxide-Modified Biochar: Experiments and DFT Investigations." Journal of Cleaner Production 403 (June). https://doi.org/10.1016/j.jclepro.2023.136821.

Cheng, Song, Saidan Zhao, Hui Guo, Baolin Xing, Yongzhi Liu, Chuanxiang Zhang, and Mingjie Ma. 2022a. "High-Efficiency Removal of Lead/Cadmium from Wastewater by MgO Modified Biochar Derived from Crofton Weed." Bioresource Technology 343 (January). https://doi.org/10.1016/j.biortech.2021.126081.

Dash, Siddhant, Smitom Swapna Borah, and Ajay S. Kalamdhad. 2021a. "Heavy Metal Pollution and Potential Ecological Risk Assessment for Surficial Sediments of Deepor Beel, India." *Ecological Indicators* 122 (March). https://doi.org/10.1016/j.ecolind.2020.107265.

El-Amier, Yasser A., Ashraf Elsayed, Mohamed A. El-Esawi, Ahmed Noureldeen, Hadeer Darwish, and Hala Fakhry. 2021. "Optimizing the Biosorption Behavior of Ludwigia Stolonifera in the Removal of Lead and Chromium Metal Ions from Synthetic Wastewater." *Sustainability (Switzerland)* 13 (11). https://doi.org/10.3390/su13116390.

Foroutan, Rauf, Seyed Jamaleddin Peighambardoust, Reza Mohammadi, Seyed Hadi Peighambardoust, and Bahman Ramavandi. 2022. "Cadmium Ion Removal from Aqueous Media Using Banana Peel Biochar/Fe3O4/ZIF-67." *Environmental Research* 211 (August). https://doi.org/10.1016/j.envres.2022.113020.

Gao, Xinyu, and Xiangchao Meng. 2021. "Photocatalysis for Heavy Metal Treatment: A Review." *Processes.* MDPI. https://doi.org/10.3390/pr9101729.

Gkika, Despina A., Athanasios C. Mitropoulos, and George Z. Kyzas. 2022. "Why Reuse Spent Adsorbents? The Latest Challenges and Limitations." *Science of the Total Environment.* Elsevier B.V. https://doi.org/10.1016/j.scitotenv.2022.153612.

Gopalakrishnan, Arthi, Rajasekar Krishnan, Sakthivel Thangavel, Gunasekaran Venugopal, and Sang Jae Kim. 2015. "Removal of Heavy Metal Ions from Pharma-Effluents Using Graphene-Oxide Nanosorbents and Study of Their Adsorption Kinetics." *Journal of Industrial and Engineering Chemistry* 30 (October):14–19. https://doi.org/10.1016/j.jiec.2015.06.005.

Haddon, Robert C. 2002. "Carbon Nanotubes." *Accounts of Chemical Research.* https://doi.org/10.1021/ar020259h.

Hayashi, Natsuki, Daiju Matsumura, Hiroyuki Hoshina, Yuji Ueki, Takuya Tsuji, Jinhua Chen, and Noriaki Seko. 2021. "Chromium(VI) Adsorption–Reduction Using a Fibrous Amidoxime-Grafted Adsorbent." *Separation and Purification Technology* 277 (December). https://doi.org/10.1016/j.seppur.2021.119536.

Hock, Pua Eng, Azrul Nurfaiz Mohd Faizal, Lawal Sirajo, and Muhammad Abbas Ahmad Zaini. 2024. "Insight into Kinetics, Equilibrium, and Thermodynamics of Malachite Green Adsorption onto Banana Peel Adsorbents." *Biomass Conversion and Biorefinery* 14 (15): 17405–21. https://doi.org/10.1007/s13399-023-04117-9.

Hoseinian, Fatemeh Sadat, Shahab Ramshini, Bahram Rezai, Elaheh Kowsari, and Mehdi Safari. 2023. "Toxic Heavy Metal Ions Removal from Wastewater by Ion Flotation Using a Nano Collector." *Minerals Engineering* 204 (December). https://doi.org/10.1016/j.mineng.2023.108380.

Hossain, Md Mokarom, Md Arif Chowdhury, Md Jawad Hasan, Md Harun Ar Rashid, Thamina Acter, M. Nuruzzaman Khan, Sheikh Mahatabuddin, and Nizam Uddin. 2021. "Heavy Metal Pollution in the Soil-Vegetable System of Tannery Estate."

Environmental Nanotechnology, Monitoring and Management 16 (December). https://doi.org/10.1016/j.enmm.2021.100557.

Huang, Hui, Hui Guan, Zhuo Qi Tian, Ming Ming Chen, Kun Kun Tian, Fang Jie Zhao, and Peng Wang. 2024. "Exposure Sources, Intake Pathways and Accumulation of Lead in Human Blood." Soil Security 15 (June). https://doi.org/10.1016/j.soisec.2024.100150.

Inam, Muhammad Ali, Rizwan Khan, Du Ri Park, Babar Aijaz Ali, Ahmed Uddin, and Ick Tae Yeom. 2018. "Influence of PH and Contaminant Redox Form on the Competitive Removal of Arsenic and Antimony from Aqueous Media by Coagulation." Minerals 8 (12). https://doi.org/10.3390/min8120574.

Irfan, Iqra, Muhammad Ali Inam, Waleed Usmani, Rashid Iftikhar, and Zaib Jahan. 2023. "Adsorptive Recovery of Phosphate Using Iron Functionalized Biochar Prepared via Co-Pyrolysis of Wheat Straw and Sewage Sludge." Environmental Technology and Innovation 32 (November). https://doi.org/10.1016/j.eti.2023.103434.

Ishaque, Waseem, Mudassir Mukhtar, and Rida Tanvir. 2023. "Pakistan's Water Resource Management: Ensuring Water Security for Sustainable Development." Frontiers in Environmental Science 11 (January). https://doi.org/10.3389/fenvs.2023.1096747.

Izhar, Tengku Nuraiti Tengku, Goh Zhi Kee, Farah Naemah Mohd Saad, Shayfull Zamree Abd Rahim, Irnis Azura Zakarya, Mohd Rizam Che Besom, Mursyidul Ibad, and Achmad Syafiuddin. 2022. "Adsorption of Hydrogen Sulfide (H2s) from Municipal Solid Waste by Using Biochars." Biointerface Research in Applied Chemistry 12 (6): 8057–69. https://doi.org/10.33263/BRIAC126.80578069.

Jumina, Yoga Priastomo, Hamid Rohma Setiawan, Mutmainah, Yehezkiel Steven Kurniawan, and Keisuke Ohto. 2020. "Simultaneous Removal of Lead(II), Chromium(III), and Copper(II) Heavy Metal Ions through an Adsorption Process Using C-Phenylcalix[4]Pyrogallolarene Material." Journal of Environmental Chemical Engineering 8 (4). https://doi.org/10.1016/j.jece.2020.103971.

Kadirvelu, K, K Thamaraiselvi, and C Namasivayam. n.d. "Removal of Heavy Metals from Industrial Wastewaters by Adsorption onto Activated Carbon Prepared from an Agricultural Solid Waste."

Karaeva, J. V., S. S. Timofeeva, A. A. Kovalev, D. A. Kovalev, M. F. Gilfanov, V. S. Grigoriev, and Y. V. Litti. 2022. "CO-PYROLYSIS of Agricultural Waste and Estimation of the Applicability of Pyrolysis in the Integrated Technology of Biorenewable Hydrogen Production." International Journal of Hydrogen Energy 47 (23): 11787–98. https://doi.org/10.1016/j.ijhydene.2022.02.057.

Kaur, Simran, and Arpita Roy. 2021a. "Bioremediation of Heavy Metals from Wastewater Using Nanomaterials." Environment, Development and Sustainability. Springer Science and Business Media B.V. https://doi.org/10.1007/s10668-020-01078-1.

Khalid, Usama, and Muhammad Ali Inam. 2024. "The Influence of Pyrolysis Temperature on the Performance of Cotton Stalk Biochar for Hexavalent Chromium Removal from

Wastewater." *Water, Air, & Soil Pollution* 235 (2): 114. https://doi.org/10.1007/s11270-024-06922-y.

Khalil, Usman, Muhammad Bilal Shakoor, Shafaqat Ali, Muhammad Rizwan, Mohammed Nasser Alyemeni, and Leonard Wijaya. 2020. "Adsorption-Reduction Performance of Tea Waste and Rice Husk Biochars for Cr(VI) Elimination from Wastewater." *Journal of Saudi Chemical Society* 24 (11): 799–810. https://doi.org/10.1016/j.jscs.2020.07.001.

Khoshnood Motlagh, Eisa, Seyedmehdi Sharifian, and Neda Asasian-Kolur. 2021. "Alkaline Activating Agents for Activation of Rice Husk Biochar and Simultaneous Bio-Silica Extraction." *Bioresource Technology Reports* 16 (December). https://doi.org/10.1016/j.biteb.2021.100853.

Kuang, Mengjie, Yisheng Shang, Gaoling Yang, Baixiong Liu, and Bin Yang. 2019. "Facile Synthesis of Hollow Mesoporous MgO Spheres via Spray-Drying with Improved Adsorption Capacity for Pb(II) and Cd(II)." *Environmental Science and Pollution Research* 26 (18): 18825–33. https://doi.org/10.1007/s11356-019-05277-w.

Kumar, Amit, Amit Kumar, M. Cabral-Pinto, Ashish K. Chaturvedi, Aftab A. Shabnam, Gangavarapu Subrahmanyam, Raju Mondal, et al. 2020. "Lead Toxicity: Health Hazards, Influence on Food Chain, and Sustainable Remediation Approaches." *International Journal of Environmental Research and Public Health.* MDPI AG. https://doi.org/10.3390/ijerph17072179.

Kumar, P. Senthil, R. Gayathri, and B. Senthil Rathi. 2021a. "A Review on Adsorptive Separation of Toxic Metals from Aquatic System Using Biochar Produced from Agro-Waste." *Chemosphere.* Elsevier Ltd. https://doi.org/10.1016/j.chemosphere.2021.131438.

Kumar, Vinay, S. K. Dwivedi, and Seungdae Oh. 2022a. "A Critical Review on Lead Removal from Industrial Wastewater: Recent Advances and Future Outlook." *Journal of Water Process Engineering.* Elsevier Ltd. https://doi.org/10.1016/j.jwpe.2021.102518.

Lakshmi, Divya, Dilipkumar Akhil, Ashokkumar Kartik, Kannappan Panchamoorthy Gopinath, Jayaseelan Arun, Amit Bhatnagar, Jörg Rinklebe, Woong Kim, and Govarthanan Muthusamy. 2021. "Artificial Intelligence (AI) Applications in Adsorption of Heavy Metals Using Modified Biochar." *Science of the Total Environment.* Elsevier B.V. https://doi.org/10.1016/j.scitotenv.2021.149623.

Lee, Han Saem, and Hyun Sang Shin. 2021. "Competitive Adsorption of Heavy Metals onto Modified Biochars: Comparison of Biochar Properties and Modification Methods." *Journal of Environmental Management* 299 (December). https://doi.org/10.1016/j.jenvman.2021.113651.

Li, An Yu, Hua Deng, Yan Hong Jiang, Cheng Hui Ye, Bi Ge Yu, Xin Lan Zhou, and Ai Ying Ma. 2020. "Superefficient Removal of Heavy Metals from Wastewater by Mg-Loaded Biochars: Adsorption Characteristics and Removal Mechanisms." *Langmuir* 36 (31): 9160–74. https://doi.org/10.1021/acs.langmuir.0c01454.

Li, Anyu, Wenzhan Ge, Lihu Liu, and Guohong Qiu. 2022a. "Preparation, Adsorption Performance and Mechanism of MgO-Loaded Biochar in Wastewater Treatment: A Review." *Environmental Research. Academic Press Inc.* https://doi.org/10.1016/j.envres.2022.113341.

Li, Anyu, Hanquan Xie, Ying Qiu, Lihu Liu, Tao Lu, Weihua Wang, and Guohong Qiu. 2022. "Resource Utilization of Rice Husk Biomass: Preparation of MgO Flake-Modified Biochar for Simultaneous Removal of Heavy Metals from Aqueous Solution and Polluted Soil." *Environmental Pollution* 310 (October). https://doi.org/10.1016/j.envpol.2022.119869.

Li, Anyu, Yue Zhang, Wenzhan Ge, Yutong Zhang, Lihu Liu, and Guohong Qiu. 2022. "Removal of Heavy Metals from Wastewaters with Biochar Pyrolyzed from MgAl-Layered Double Hydroxide-Coated Rice Husk: Mechanism and Application." *Bioresource Technology* 347 (March). https://doi.org/10.1016/j.biortech.2021.126425.

Liang, Hai, Wanting Wang, Haiyan Liu, Xinzhong Deng, Dan Zhang, Yuxuan Zou, and Xuehua Ruan. 2023. "Porous MgO-Modified Biochar Adsorbents Fabricated by the Activation of Mg(NO3)2 for Phosphate Removal: Synergistic Enhancement of Porosity and Active Sites." *Chemosphere* 324 (May). https://doi.org/10.1016/j.chemosphere.2023.138320.

Ling, Li Li, Wu Jun Liu, Shun Zhang, and Hong Jiang. 2017. "Magnesium Oxide Embedded Nitrogen Self-Doped Biochar Composites: Fast and High-Efficiency Adsorption of Heavy Metals in an Aqueous Solution." *Environmental Science and Technology* 51 (17): 10081–89. https://doi.org/10.1021/acs.est.7b02382.

Liu, Hongbo, Jinhua Shan, Zhongbing Chen, and Eric Lichtfouse. 2021. "Efficient Recovery of Phosphate from Simulated Urine by Mg/Fe Bimetallic Oxide Modified Biochar as a Potential Resource." *Science of the Total Environment* 784 (August). https://doi.org/10.1016/j.scitotenv.2021.147546.

Liu, Tianqi, Yelly Lawluvy, Yang Shi, Joshua O. Ighalo, Yide He, Yongjun Zhang, and Pow Seng Yap. 2022. "Adsorption of Cadmium and Lead from Aqueous Solution Using Modified Biochar: A Review." *Journal of Environmental Chemical Engineering. Elsevier Ltd.* https://doi.org/10.1016/j.jece.2021.106502.

Luna-Lama, Fernando, Julián Morales, and Alvaro Caballero. 2021. "Biomass Porous Carbons Derived from Banana Peel Waste as Sustainable Anodes for Lithium-Ion Batteries." *Materials* 14 (20). https://doi.org/10.3390/ma14205995.

Ma, Anthony, Ahmad Abushaikha, Stephen J. Allen, and Gordon McKay. 2019. "Ion Exchange Homogeneous Surface Diffusion Modelling by Binary Site Resin for the Removal of Nickel Ions from Wastewater in Fixed Beds." *Chemical Engineering Journal* 358 (February):1–10. https://doi.org/10.1016/j.cej.2018.09.135.

Mahmoud, Mohamed E., Nesma A. Fekry, and Amir M. Abdelfattah. 2020. "A Novel Nanobiosorbent of Functionalized Graphene Quantum Dots from Rice Husk with Barium Hydroxide for Microwave Enhanced Removal of Lead (II) and Lanthanum

(III)." *Bioresource Technology* 298 (February). https://doi.org/10.1016/j.biortech.2019.122514.

Masoud, Mamdouh S., Sawsan S. Haggag, Hany Fathy Heiba, Omayma H. Abd El-Hamed, Nabil S. Habila, Ibrahim A.M. Abdel-hamid, and Laila A. Mohamed. 2023. "Comparative Adsorption Affinities of Nano-Metal Oxides Towards Cr(VI): Synthesis, Characterization, Kinetics, Isotherms, Thermodynamic and Techno-Economics Study." *Environmental Processes* 10 (2). https://doi.org/10.1007/s40710-023-00651-w.

Memon, Muhammad Jaffar, & Ashfaque, Ahmed Jhatial, Ali Murtaza, Muhammad Saleem Raza, and Karim Bux Phulpoto. n.d. "Production of Eco-Friendly Concrete Incorporating Rice Husk Ash and Polypropylene Fibres." https://doi.org/10.1007/s11356-021-13418-3/Published.

Menya, E, P W Olupot, & H Storz, & M Lubwama, and Y Kiros. n.d. "Synthesis and Evaluation of Activated Carbon from Rice Husks for Removal of Humic Acid from Water." https://doi.org/10.1007/s13399-020-01158-2/Published.

Menya, E., P. W. Olupot, H. Storz, M. Lubwama, Y. Kiros, and M. J. John. 2020. "Optimization of Pyrolysis Conditions for Char Production from Rice Husks and Its Characterization as a Precursor for Production of Activated Carbon." *Biomass Conversion and Biorefinery* 10 (1): 57–72. https://doi.org/10.1007/s13399-019-00399-0.

Moradi, Mahsa, and Gholamreza Moussavi. 2019. "Enhanced Treatment of Tannery Wastewater Using the Electrocoagulation Process Combined with UVC/VUV Photoreactor: Parametric and Mechanistic Evaluation." *Chemical Engineering Journal* 358 (February):1038–46. https://doi.org/10.1016/j.cej.2018.10.069.

Mubarak, Nabisab, Manimaran Thobashinni, Ezzat Abdullah, and Jaya Sahu. 2016. "Comparative Kinetic Study of Removal of Pb2+ Ions and Cr3+ Ions from Waste Water Using Carbon Nanotubes Produced Using Microwave Heating." *C* 2 (1): 7. https://doi.org/10.3390/c2010007.

Muthukrishnan, Shravan, Souradeep Gupta, and Harn Wei Kua. 2019. "Application of Rice Husk Biochar and Thermally Treated Low Silica Rice Husk Ash to Improve Physical Properties of Cement Mortar." *Theoretical and Applied Fracture Mechanics* 104 (December). https://doi.org/10.1016/j.tafmec.2019.102376.

Nag, Rajat, and Enda Cummins. 2022. "Human Health Risk Assessment of Lead (Pb) through the Environmental-Food Pathway." *Science of the Total Environment* 810 (March). https://doi.org/10.1016/j.scitotenv.2021.151168.

Nasrollahi, Zahra, Mohadeseh sadat Hashemi, Saeed Bameri, and Vahid Mohamad Taghvaee. 2020. "Environmental Pollution, Economic Growth, Population, Industrialization, and Technology in Weak and Strong Sustainability: Using STIRPAT Model." *Environment, Development and Sustainability* 22 (2): 1105–22. https://doi.org/10.1007/s10668-018-0237-5.

Nath, B. K., C. Chaliha, and E. Kalita. 2019. "Iron Oxide Permeated Mesoporous Rice-Husk Nanobiochar (IPMN) Mediated Removal of Dissolved Arsenic (As): Chemometric Modelling and Adsorption Dynamics." *Journal of Environmental Management* 246 (September):397–409. https://doi.org/10.1016/j.jenvman.2019.06.008.

Ngankam, Eric Sakué, Lemankreo Dai-Yang, Baissassou Debina, Abdellaziz Baçaoui, Abdelrani Yaacoubi, and Abdoul Ntieche Rahman. 2020. "Preparation and Characterization of Magnetic Banana Peels Biochar for Fenton Degradation of Methylene Blue." *Materials Sciences and Applications* 11 (06): 382–400. https://doi.org/10.4236/msa.2020.116026.

Ni, Bing Jie, Qi Su Huang, Chen Wang, Tian Yi Ni, Jing Sun, and Wei Wei. 2019. "Competitive Adsorption of Heavy Metals in Aqueous Solution onto Biochar Derived from Anaerobically Digested Sludge." *Chemosphere* 219 (March):351–57. https://doi.org/10.1016/j.chemosphere.2018.12.053.

Nithya, R., and P. N. Sudha. 2017. "Removal of Heavy Metals from Tannery Effluent Using Chitosan-g-Poly(Butyl Acrylate)/Bentonite Nanocomposite as an Adsorbent." *Textiles and Clothing Sustainability* 2 (1). https://doi.org/10.1186/s40689-016-0018-1.

Noreen, Uzma, Zahoor Ahmed, Aliya Khalid, Alessandra Di Serafino, Ume Habiba, Farzand Ali, and Majid Hussain. 2019. "Water Pollution and Occupational Health Hazards Caused by the Marble Industries in District Mardan, Pakistan." *Environmental Technology and Innovation* 16 (November). https://doi.org/10.1016/j.eti.2019.100470.

Oladipo, Akeem Adeyemi, Edith Odinaka Ahaka, and Mustafa Gazi. 2019a. "High Adsorptive Potential of Calcined Magnetic Biochar Derived from Banana Peels for Cu^{2+}, Hg^{2+}, and Zn^{2+} Ions Removal in Single and Ternary Systems." *Environmental Science and Pollution Research* 26 (31): 31887–99. https://doi.org/10.1007/s11356-019-06321-5.

Pan, Z. F., and L. An. 2019. "Removal of Heavy Metal from Wastewater Using Ion Exchange Membranes." In *Applications of Ion Exchange Materials in the Environment*, 25–46. Springer International Publishing. https://doi.org/10.1007/978-3-030-10430-6_2.

Pandey, Lalit M. 2021. "Surface Engineering of Nano-Sorbents for the Removal of Heavy Metals: Interfacial Aspects." *Journal of Environmental Chemical Engineering* 9 (1). https://doi.org/10.1016/j.jece.2020.104586.

Phys Sci, Adsorbent, Abu Sayid Mia, Uzzal Ali, Mafizur Rahman, and Zahangir Alam. 2020. "Physical Science & Biophysics Journal Committed to Create Value for Researchers Removal of Heavy Metals from Tannery Wastewater by Using Sawdust and Spent Tea Leaves as an Removal of Heavy Metals from Tannery Wastewater by Using Sawdust and Spent Tea Leaves as an Adsorbent."

Poznanović Spahić, Maja M., Sanja M. Sakan, Bojan M. Glavaš-Trbić, Pavle I. Tančić, Sandra B. Škrivanj, Jovan R. Kovačević, and Dragan D. Manojlović. 2019. "Natural

and Anthropogenic Sources of Chromium, Nickel and Cobalt in Soils Impacted by Agricultural and Industrial Activity (Vojvodina, Serbia)." *Journal of Environmental Science and Health - Part A Toxic/Hazardous Substances and Environmental Engineering* 54 (3): 219–30. https://doi.org/10.1080/10934529.2018.1544802.

Priya, A. K., V. Yogeshwaran, Saravanan Rajendran, Tuan K.A. Hoang, Matias Soto-Moscoso, Ayman A. Ghfar, and Chinna Bathula. 2022a. "Investigation of Mechanism of Heavy Metals (Cr6+, Pb2+& Zn2+) Adsorption from Aqueous Medium Using Rice Husk Ash: Kinetic and Thermodynamic Approach." *Chemosphere* 286 (January). https://doi.org/10.1016/j.chemosphere.2021.131796.

Qayoom, U., S. U. Bhat, I. Ahmad, and A. Kumar. 2022. "Assessment of Potential Risks of Heavy Metals from Wastewater Treatment Plants of Srinagar City, Kashmir." *International Journal of Environmental Science and Technology* 19 (9): 9027–46. https://doi.org/10.1007/s13762-021-03612-8.

Qi, Xin, Hua Yin, Minghan Zhu, Xiaolong Yu, Pengling Shao, and Zhi Dang. 2022. "MgO-Loaded Nitrogen and Phosphorus Self-Doped Biochar: High-Efficient Adsorption of Aquatic Cu2+, Cd2+, and Pb2+ and Its Remediation Efficiency on Heavy Metal Contaminated Soil." *Chemosphere* 294 (May). https://doi.org/10.1016/j.chemosphere.2022.133733.

Qin, Xianxian, Jixin Luo, Zhigao Liu, and Yunlin Fu. 2020. "Preparation and Characterization of Mgo-Modified Rice Straw Biochars." *Molecules* 25 (23). https://doi.org/10.3390/molecules25235730.

Rajendran, Saravanan, A. K. Priya, P. Senthil Kumar, Tuan K.A. Hoang, Karthikeyan Sekar, Kar Yeen Chong, Kuan Shiong Khoo, Hui Suan Ng, and Pau Loke Show. 2022. "A Critical and Recent Developments on Adsorption Technique for Removal of Heavy Metals from Wastewater-A Review." *Chemosphere* 303 (September). https://doi.org/10.1016/j.chemosphere.2022.135146.

Rani, K., T. Gomathi, K. Vijayalakshmi, M. Saranya, and P. N. Sudha. 2019. "Banana Fiber Cellulose Nano Crystals Grafted with Butyl Acrylate for Heavy Metal Lead (II) Removal." *International Journal of Biological Macromolecules* 131 (June):461–72. https://doi.org/10.1016/j.ijbiomac.2019.03.064.

Raouf MS, Abdel, and Abdul Raheim ARM. 2016. "Removal of Heavy Metals from Industrial Wastewater by Biomass-Based Materials: A Review." *Journal of Pollution Effects & Control* 05 (01). https://doi.org/10.4172/2375-4397.1000180.

Rathi, B. Senthil, P. Senthil Kumar, and Dai Viet N. Vo. 2021. "Critical Review on Hazardous Pollutants in Water Environment: Occurrence, Monitoring, Fate, Removal Technologies and Risk Assessment." *Science of the Total Environment* 797 (November). https://doi.org/10.1016/j.scitotenv.2021.149134.

Saeed, Shagufta, Ubaid Ur Rehman Baig, Muhammad Tayyab, Imran Altaf, Muhammad Irfan, Syed Qasim Raza, Fareeha Nadeem, and Tahir Mehmood. 2021. "Valorization of Banana Peels Waste into Biovanillin and Optimization of Process Parameters Using Submerged Fermentation." *Biocatalysis and Agricultural Biotechnology* 36 (September). https://doi.org/10.1016/j.bcab.2021.102154.

Sajad, Muhammad Anwar, Muhammad Saleem Khan, Saraj Bahadur, Abdul Naeem, Hazrat Ali, Farwa Batool, Muhammad Shuaib, Muhammad Anwar Saleem Khan, and Saneya Batool. 2020. "Evaluation of Chromium Phytoremediation Potential of Some Plant Species of Dir Lower, Khyber Pakhtunkhwa, Pakistan." *Acta Ecologica Sinica* 40 (2): 158–65. https://doi.org/10.1016/J.CHNAES.2019.12.002.

Saleem, Muhammed, and Mohammed Tariq Saeed. 2020. "Potential Application of Waste Fruit Peels (Orange, Yellow Lemon and Banana) as Wide Range Natural Antimicrobial Agent." *Journal of King Saud University - Science* 32 (1): 805–10. https://doi.org/10.1016/j.jksus.2019.02.013.

Saleh, Tawfik A., and Islam Ali. 2018. "Synthesis of Polyamide Grafted Carbon Microspheres for Removal of Rhodamine B Dye and Heavy Metals." *Journal of Environmental Chemical Engineering* 6 (4): 5361–68. https://doi.org/10.1016/j.jece.2018.08.033.

Saleh, Tawfik A., Asma M. Elsharif, Sarah Asiri, Abdul Rashid I. Mohammed, and H. Dafalla. 2020. "Synthesis of Carbon Nanotubes Grafted with Copolymer of Acrylic Acid and Acrylamide for Phenol Removal." *Environmental Nanotechnology, Monitoring and Management* 14 (December). https://doi.org/10.1016/j.enmm.2020.100302.

Saleh, Tawfik A., Mujahid Mustaqeem, and Mazen Khaled. 2022. "Water Treatment Technologies in Removing Heavy Metal Ions from Wastewater: A Review." *Environmental Nanotechnology, Monitoring and Management.* Elsevier B.V. https://doi.org/10.1016/j.enmm.2021.100617.

Samuel, Melvin S., Sk Sheriff Shah, Jayanta Bhattacharya, Kalidass Subramaniam, and N. D. Pradeep Singh. 2018. "Adsorption of Pb(II) from Aqueous Solution Using a Magnetic Chitosan/Graphene Oxide Composite and Its Toxicity Studies." *International Journal of Biological Macromolecules* 115 (August):1142–50. https://doi.org/10.1016/j.ijbiomac.2018.04.185.

Sanka, P. M., M. J. Rwiza, and K. M. Mtei. 2020a. "Removal of Selected Heavy Metal Ions from Industrial Wastewater Using Rice and Corn Husk Biochar." *Water, Air, and Soil Pollution* 231 (5). https://doi.org/10.1007/s11270-020-04624-9.

Saravanan, Praveen, Jegan Josephraj, & Bhagavathi, Pushpa Thillainayagam, and Gokulan Ravindiran. n.d. "Evaluation of the Adsorptive Removal of Cationic Dyes by Greening Biochar Derived from Agricultural Bio-Waste of Rice Husk." https://doi.org/10.1007/s13399-021-01415-y/Published.

Scapin, Enelise, Gabriela Pereira da Silva Maciel, Allan Dos Santos Polidoro, Eliane Lazzari, Edilson Valmir Benvenutti, Tiago Falcade, and Rosângela Assis Jacques. 2021. "Activated Carbon from Rice Husk Biochar with High Surface Area." *Biointerface Research in Applied Chemistry* 11 (3): 10265–77. https://doi.org/10.33263/BRIAC113.1026510277.

Sepehri, Arsalan, Mohammad Hossein Sarrafzadeh, and Maryam Avateffazeli. 2020. "Interaction between Chlorella Vulgaris and Nitrifying-Enriched Activated Sludge

in the Treatment of Wastewater with Low C/N Ratio." *Journal of Cleaner Production* 247 (February). https://doi.org/10.1016/j.jclepro.2019.119164.

Shadreck, Mandina, and Tawanda Mugadza. 2013. "African Journal of Pure and Applied Chemistry Chromium, an Essential Nutrient and Pollutant: A Review" 7 (9): 310–17. https://doi.org/10.5897/AJPAC2013.

Shafiq, Muhammad, Abdulrahman Ali Alazba, and Muhammad Tahir Amin. 2023. "Preparation of ZnMgAl-Layered Double Hydroxide and Rice Husk Biochar Composites for Cu(II) and Pb(II) Ions Removal from Synthetic Wastewater." *Water (Switzerland)* 15 (12). https://doi.org/10.3390/w15122207.

Sharma, Anket, Dhriti Kapoor, Junfeng Wang, Babar Shahzad, Vinod Kumar, Aditi Shreeya Bali, Shivam Jasrotia, Bingsong Zheng, Huwei Yuan, and Daoliang Yan. 2020. "Chromium Bioaccumulation and Its Impacts on Plants: An Overview." *Plants*. MDPI AG. https://doi.org/10.3390/plants9010100.

Shi, Junxian, Xiaoliang Fan, Daniel C.W. Tsang, Fei Wang, Zhengtao Shen, Deyi Hou, and Daniel S. Alessi. 2019. "Removal of Lead by Rice Husk Biochars Produced at Different Temperatures and Implications for Their Environmental Utilizations." *Chemosphere* 235 (November):825–31. https://doi.org/10.1016/j.chemosphere.2019.06.237.

Shi, Qingliang, Hua Zhang, Asfandyar Shahab, Honghu Zeng, Huiting Zeng, Aziz Ur Rahim Bacha, Iqra Nabi, Jamil Siddique, and Habib Ullah. 2021a. "Efficient Performance of Magnesium Oxide Loaded Biochar for the Significant Removal of Pb^{2+} and Cd^{2+} from Aqueous Solution." *Ecotoxicology and Environmental Safety* 221 (September). https://doi.org/10.1016/j.ecoenv.2021.112426.

Shrestha, Rakesh, Sagar Ban, Sijan Devkota, Sudip Sharma, Rajendra Joshi, Arjun Prasad Tiwari, Hak Yong Kim, and Mahesh Kumar Joshi. 2021a. "Technological Trends in Heavy Metals Removal from Industrial Wastewater: A Review." *Journal of Environmental Chemical Engineering*. Elsevier Ltd. https://doi.org/10.1016/j.jece.2021.105688.

Shukla, Abhimati, Zainab Mahmood, and Lalit Kumar Singh. 2021. "Studies on Recovery of Heavy Metals from Tannery Wastewater." *International Journal of Engineering, Science and Technology* 13 (1): 76–80. https://doi.org/10.4314/ijest.v13i1.11s.

Singh, N. B., Garima Nagpal, Sonal Agrawal, and Rachna. 2018. "Water Purification by Using Adsorbents: A Review." *Environmental Technology and Innovation*. Elsevier B.V. https://doi.org/10.1016/j.eti.2018.05.006.

Sk, Wahedur, and Shouvik Chattopadhyay. 2022. "An Overview of the Synthesis and Structures Lead(II) and Mercury(II) Complexes with Diamine-Based Bis-Pyridine Schiff Base Ligands." *Results in Chemistry*. Elsevier B.V. https://doi.org/10.1016/j.rechem.2022.100639.

Sun, Hong, Jason Brocato, and Max Costa. 2015. "Oral Chromium Exposure and Toxicity." *Current Environmental Health Reports*. Springer. https://doi.org/10.1007/s40572-015-0054-z.

Sun, Ying tao, Jia dong Chen, Zhen hua Wei, Yue kai Chen, Chun lei Shao, and Jian feng Zhou. 2023. "Copper Ion Removal from Aqueous Media Using Banana Peel Biochar/Fe3O4/Branched Polyethyleneimine." *Colloids and Surfaces A: Physicochemical and Engineering Aspects* 658 (February). https://doi.org/10.1016/j.colsurfa.2022.130736.

Sun, Yongjun, Shengbao Zhou, Shu Yuan Pan, Sichen Zhu, Yang Yu, and Huaili Zheng. 2020. "Performance Evaluation and Optimization of Flocculation Process for Removing Heavy Metal." *Chemical Engineering Journal* 385 (April). https://doi.org/10.1016/j.cej.2019.123911.

Tang, Yao, Md Samrat Alam, Kurt O. Konhauser, Daniel S. Alessi, Shengnan Xu, Wei Jun Tian, and Yang Liu. 2019. "Influence of Pyrolysis Temperature on Production of Digested Sludge Biochar and Its Application for Ammonium Removal from Municipal Wastewater." *Journal of Cleaner Production* 209 (February):927–36. https://doi.org/10.1016/j.jclepro.2018.10.268.

Tariq, Waheed. 2019. "Removal Of Heavy Metals From Chemical Industrial Wastewater Using Agro Based Bio-Sorbents." https://doi.org/10.26480/acmy.02.2018.09.14.

Thomas, Paul, Chin Wei Lai, and Mohd Rafie Bin Johan. 2019. "Recent Developments in Biomass-Derived Carbon as a Potential Sustainable Material for Super-Capacitor-Based Energy Storage and Environmental Applications." *Journal of Analytical and Applied Pyrolysis.* Elsevier B.V. https://doi.org/10.1016/j.jaap.2019.03.021.

Thuan, Tran Van, Bui Thi Phuong Quynh, Trinh Duy Nguyen, Van Thi Thanh Ho, and Long Giang Bach. 2017. "Response Surface Methodology Approach for Optimization of Cu2+, Ni2+ and Pb2+ Adsorption Using KOH-Activated Carbon from Banana Peel." *Surfaces and Interfaces* 6 (March):209–17. https://doi.org/10.1016/j.surfin.2016.10.007.

Tran, Dinh Trinh, Thuy Duong Pham, Viet Cuong Dang, Thanh Dong Pham, Minh Viet Nguyen, Nhat Minh Dang, Minh Ngoc Ha, Van Noi Nguyen, and Long D. Nghiem. 2022a. "A Facile Technique to Prepare MgO-Biochar Nanocomposites for Cationic and Anionic Nutrient Removal." *Journal of Water Process Engineering* 47 (June). https://doi.org/10.1016/j.jwpe.2022.102702.

Usmani, Waleed, Muhammad Ali Inam, Rashid Iftikhar, Iqra Irfan, Rabia Adnan, Muhammad Bilal Khan Niazi, Rizwan Khan, and Muhammad Hassan. 2023. "Efficient Removal of Hexavalent Chromium Cr (VI) Using Magnesium-Iron Layered Double Hydroxide Supported on Orange Peel (Mg-Fe LDH@OPP): A Synthetic Experimental and Mechanism Studies." *Journal of Water Process Engineering* 55 (October). https://doi.org/10.1016/j.jwpe.2023.104233.

Verger, Louisiane, Olivier Dargaud, Mathieu Chassé, Nicolas Trcera, Gwenaëlle Rousse, and Laurent Cormier. 2018. "Synthesis, Properties and Uses of Chromium-Based Pigments from the Manufacture de Sèvres." *Journal of Cultural Heritage* 30 (March):26–33. https://doi.org/10.1016/j.culher.2017.09.012.

Wang, Li, Chengxiang Shi, Lun Pan, Xiangwen Zhang, and Ji Jun Zou. 2020. "Rational Design, Synthesis, Adsorption Principles and Applications of Metal Oxide

Adsorbents: A Review." *Nanoscale. Royal Society of Chemistry.* https://doi.org/10.1039/c9nr09274a.

Wang, Ting, Hongwen Sun, Xinhao Ren, Bing Li, and Hongjun Mao. 2018. "Adsorption of Heavy Metals from Aqueous Solution by UV-Mutant Bacillus Subtilis Loaded on Biochars Derived from Different Stock Materials." *Ecotoxicology and Environmental Safety* 148 (February):285–92. https://doi.org/10.1016/j.ecoenv.2017.10.039.

Witkowska, Danuta, Joanna Słowik, and Karolina Chilicka. 2021. "Review Heavy Metals and Human Health: Possible Exposure Pathways and the Competition for Protein Binding Sites." *Molecules. MDPI.* https://doi.org/10.3390/molecules26196060.

Xiang, Jiangxin, Qintie Lin, Shuailong Cheng, Jianlong Guo, Xiaosheng Yao, Qianjun Liu, Guangcai Yin, and Dingfa Liu. 2018a. "Enhanced Adsorption of Cd(II) from Aqueous Solution by a Magnesium Oxide–Rice Husk Biochar Composite." *Environmental Science and Pollution Research* 25 (14): 14032–42. https://doi.org/10.1007/s11356-018-1594-1.

Xiao, Jingjiang, Haiping Long, Xuemei He, Guoyu Chen, Tao Yuan, Yi Liu, and Qiaoling Xu. 2024. "Synthesis of MgO-Coated Canna Biochar and Its Application in the Treatment of Wastewater Containing Phosphorus." *Water (Switzerland)* 16 (6). https://doi.org/10.3390/w16060873.

Xu, Yingjie, Hongying Xia, Qi Zhang, Guiyu Jiang, Wuchen Cai, and Wenhai Hu. 2022a. "Adsorption of Cadmium(II) in Wastewater by Magnesium Oxide Modified Biochar." *Arabian Journal of Chemistry* 15 (9). https://doi.org/10.1016/j.arabjc.2022.104059.

Yang, Jie, Qing Wei, Changan Tian, Dong Li, Hongming Li, Guangchao Qin, Kunhong Hu, and Qinyan Zhang. 2023. "Preparation of Biomass Carbon Composites MgO@ZnO@BC and Its Adsorption and Removal of Cu(II) and Pb(II) in Wastewater." *Molecules* 28 (19). https://doi.org/10.3390/molecules28196982.

Younas, Fazila, Nabeel Khan Niazi, Irshad Bibi, Muhammad Afzal, Khalid Hussain, Muhammad Shahid, Zubair Aslam, Safdar Bashir, Muhammad Mahroz Hussain, and Jochen Bundschuh. 2022. "Constructed Wetlands as a Sustainable Technology for Wastewater Treatment with Emphasis on Chromium-Rich Tannery Wastewater." *Journal of Hazardous Materials* 422 (January). https://doi.org/10.1016/j.jhazmat.2021.126926.

Yu, Deyou, Lili Wang, and Minghua Wu. 2018. "Simultaneous Removal of Dye and Heavy Metal by Banana Peels Derived Hierarchically Porous Carbons." *Journal of the Taiwan Institute of Chemical Engineers* 93 (December):543–53. https://doi.org/10.1016/j.jtice.2018.08.038.

Yu, Hong, Zheng Zhang, Ying Zhang, Ping Fan, Beidou Xi, and Wenbing Tan. 2021. "Metal Type and Aggregate Microenvironment Govern the Response Sequence of Speciation Transformation of Different Heavy Metals to Microplastics in Soil." *Science of the Total Environment* 752 (January). https://doi.org/10.1016/j.scitotenv.2020.141956.

Yurekli, Yilmaz. 2016. "Removal of Heavy Metals in Wastewater by Using Zeolite Nano-Particles Impregnated Polysulfone Membranes." *Journal of Hazardous Materials* 309 (May):53–64. https://doi.org/10.1016/j.jhazmat.2016.01.064.

Zhang, Jingzhuo, Deyi Hou, Zhengtao Shen, Fei Jin, David O'Connor, Shizhen Pan, Yong Sik Ok, Daniel C.W. Tsang, Nanthi S. Bolan, and Daniel S. Alessi. 2020a. "Effects of Excessive Impregnation, Magnesium Content, and Pyrolysis Temperature on MgO-Coated Watermelon Rind Biochar and Its Lead Removal Capacity." *Environmental Research* 183 (April). https://doi.org/10.1016/j.envres.2020.109152.

Zhang, Linlin, Wancheng Zhu, Heng Zhang, Siwei Bi, and Qiang Zhang. 2014. "Hydrothermal-Thermal Conversion Synthesis of Hierarchical Porous MgO Microrods as Efficient Adsorbents for Lead(II) and Chromium(vi) Removal." *RSC Advances* 4 (58): 30542–50. https://doi.org/10.1039/c4ra03971h.

Zhang, Yue, and Xiumei Duan. 2020. "Chemical Precipitation of Heavy Metals from Wastewater by Using the Synthetical Magnesium Hydroxy Carbonate." *Water Science and Technology* 81 (6): 1130–36. https://doi.org/10.2166/wst.2020.208.

Zhao, Changqing, and Wuyong Chen. 2019. "A Review for Tannery Wastewater Treatment: Some Thoughts under Stricter Discharge Requirements." *Environmental Science and Pollution Research* 26 (25): 26102–11. https://doi.org/10.1007/s11356-019-05699-6.

Zhao, Meiduo, Jing Xu, Ang Li, Yayuan Mei, Xiaoyu Ge, Xiaolin Liu, Lanping Wei, and Qun Xu. 2020. "Multiple Exposure Pathways and Urinary Chromium in Residents Exposed to Chromium." *Environment International* 141 (August). https://doi.org/10.1016/j.envint.2020.105753.

Zhao, Yang, Wenkai Chang, Zhiding Huang, Xugen Feng, Lin Ma, Xiaoxia Qi, and Zenghe Li. 2017. "Enhanced Removal of Toxic Cr(VI) in Tannery Wastewater by Photoelectrocatalysis with Synthetic TiO 2 Hollow Spheres." *Applied Surface Science* 405 (May):102–10. https://doi.org/10.1016/j.apsusc.2017.01.306.

Zhu, Danchen, Yingquan Chen, Haiping Yang, Shenghua Wang, Xianhua Wang, Shihong Zhang, and Hanping Chen. 2020a. "Synthesis and Characterization of Magnesium Oxide Nanoparticle-Containing Biochar Composites for Efficient Phosphorus Removal from Aqueous Solution." *Chemosphere* 247 (May). https://doi.org/10.1016/j.chemosphere.2020.125847.

Tayyaba Thesis